Master Thesis

Memory Diodes Based on

Ferroelectric:Fluorinated Semiconducting Polymer Blends

vorgelegt am 30.11.2018

von

Minye Jin

Matrikelnummer: 4360981

Master of Science, Sustainable Materials -Polymer Sciences

Fakultät für Chemie und Pharmazie der Albert-Ludwigs-Universität Freiburg

Molekulare Elektronik

Max-Planck-Institut für Polymerforschung

Der Erstgutachter: Herr Prof. Dr. Andreas Walther

Der zweite Gutachter: Herr Prof. Dr. Paul Blom

Einreichung der schriftlichen Masterarbeit

im Studiengang M.Sc. Sustainable Materials

Name der/des Studentin/en: ……

Matrikelnummer: ……

Erklärung

Hiermit versichere ich, dass ich die Masterarbeit selbstständig verfasst und keine anderen als die von mir angegebenen Quellen und Hilfsmittel benutzt habe. Alle Stellen, die wörtlich, oder sinngemäß aus an deren Werken entnommenen sind, habe ich als solche gekennzeichnet. Alle Abbildungen enthalten nur die originalen Daten und sind in keinem Fall inhaltsverändernder Bildbearbeitungunterzogen worden. Dieabgegebene schriftliche und elektronische Fassung sind identisch. Weiterhin versichere ich, dass die Arbeit no ch nicht ande rweitig als Masterarbeit eingereicht wurde.

..... …… ……

Ort/Datum Unterschrift der/des Studentin/en

Abbreviations

AFM	atomic force micrographs
DOBAMBC	p-decyloxybenzylidene p'-amino 2-methyl butyl cinnamate
T_c	Curie temperature
P_r	The remnant polarization
Ba	Barium
E_c	coercive field
F8PT	poly[(9,9-dioctylfluorenyl-2,7-diyl)-alt-co-(1,4-benzo-{2,1',3}-thiadiazole)]
PVC	poly(vinyl chloride)
PFO	poly(9'9-dioctyl-fluorene)
PMMA	poly(methyl methacrylate)
PVDF	poly(vinylidene fluoride)
PCDTBT	poly[N-9'-heptadecanyl-2,7-carbazole-alt-5,5-(4',7'-di-2-thienyl-2',1',3'-benzothiadiazole)]
PTFE	polytetrafluoroethylene
PEDOT:PSS	poly(3,4-ethylenedioxythiophene)-poly(styrenesulfonate)
SF	semifluoroalkyl
TrFE	trifluoroethylene
TeFE	tetrafluoroethylene
THF	tetrahydrofuran
DMSO	dimethyl sulfoxide
Cr	Chromium
Al	Aluminum
HOMO	highest occupied molecular orbital
LUMO	lowest unoccupied molecular orbital
Si	Silicon
Ge	Germanium
LEDs	light-emitting diodes
UCST	upper critical dissolution temperature
LCST	lower critical dissolution temperature
rir-P3HT	regio-irregular poly(3-hexylthiophene)
SEM	scanning electron microscope

Table of content

Summary

Organic non-volatile memory device based on phase-separated blends of ferroelectric and semiconducting polymer arouses attention in the field of information storage for its flexible processibility. So far, only completely phase-separated systems have been investigated. Here, we reveal memory devices fabricated with semifluoroalkyl-poly[N-9'-heptadecanyl-2,7-carbazole-alt-5,5-(4',7'-di-2-thienyl-2',1',3'-benzothiadiazole)] (SF-PCDTBT) and hexyl-poly[N-9'-heptadecanyl-2,7-carbazole-alt-5,5-(4',7'-di-2-thienyl-2',1',3'-benzothiadiazole)] (Hexyl-PCDTBT). The morphology of the SF-PCDTBT based polymer blends film deviates strongly from the previous systems. A better miscibility of SF-PCDTBT and poly[(vinylidenefluoride-co-trifluoroethylene] [P(VDF-TrFE)] was observed. The ON-state current of the semifuorinated semiconductor based polymer blends film memory devices is about three orders of magnitude higher than the OFF-state current and the device performance is comparable to the poly(9'9-dioctyl-fluorene) (PFO) based devices. Moreover, electroluminescence characterization demonstrates the recombination of electrons and holes in the SF-PCDTBT semiconductor based memory diode.

Zusamenfassung

Der organisch nicht-flüchtige Datenspeicher, der auf phasengetrennten, ferroelektrischen und halbleitenden Polymerbeschichtungen basiert, erregt aufgrund seiner flexiblen Verarbeitbarkeit die Aufmerksamkeiten im Bereich der Datenspeicherung. Bis jetzt wurde nur das vollständig phasengetrennte System untersucht. Hier stellen wir einen Datenspeicher vor, der mit poly(Fluoro-Thiophen-Benzothiadiazol)-basierten Halbleitern hegestellt wird. Die Polymerbeschichtungen, die auf semifluorierten Alkylseitenketten-modifiezierten Halbleitern basiert, weist eine teil-integrierte phasengetrennte Morphologie auf. Das An/Aus-Verhältnis des halbleitenden, ferroelektrischen polymerbeschichten Datenspeichers ist um drei Größenordnungen höher und besitzt vergleichbare Leistungsfähigkeit. Darüber hinaus zeigt eine Charakterisierung durch Elektrolumineszenz die Rekombination von Elektronen und Löchern in der SF-Speicherdiode auf.

1 Introduction

Non-volatile memory devices, which utilizes a physical property that displays hysteresis in answer to an applied electric field to store information[1], are a more promising memory technology for its non-volatility and rewritability. Many endeavors have been put in developing memory devices for a variety of applications. Organic non-volatile memory devices founded on ferroelectricity plays an important role in memory technology for its reversible spontaneous polarization[2]. In order to achieve non-destructive read-out purpose, resistive switching is requested. In this thesis, a solution-processed ferroelectric and semiconducting polymer blends film is used combining both ferroelectricity and conductivity in the device.

1.1 Ferroelectricity

In the1920s the ferroelectricity was firstly discovered[1][3], showing a similarity between the electrical properties of ferroelectrics and the magnetic properties of ferromagnets. The polarization P(or the dielectric displacement D) follows with a varied electric field that is analogical the magnetization M(or the magnetic field B) changing with the magnetizing field H. Comparing with most dielectric materials ferroelectrics present an electric hysteresis loop in the plot of polarization versus electric field. A spontaneous polarization exists inside the ferroelectric materials without the external field.

An electric hysteresis, however, should not be convinced as the only way to identify ferroelectric. Some permeable medium with non-thermal-equilibrium charges shows this property as well, but removing the external field will result in the charges turn in to equilibrium state[4]. Crystalline materials inside which the intrinsic dipole moment well oriented indicate spontaneous polarization while amorphous materials don't bring about ferroelectricity because of the random-oriented dipole moments. In some crystal structure, the crystal symmetry can give rise to cancellation of dipole moments and therefore result in non-ferroelectricity. The degree of symmetry should not be excessive. The proper coupling of a net permanent moment is also demanded by the ferroelectricity[5].

Phase transition has been observed in many ferroelectrics[6]. T_c is described as a critical point for the phase transition from ferromagnetic state to paramagnetic state. The term Curie temperature is analogous to the elevated temperature T_0 at which the materials transit from ferroelectric state to the paraelectric state. Both first- and second-order phase changes take place[7]. A first-order phase transition is a sudden process that the lattice parameters change discontinuously. The latent heat is released at the transit point, accompanied by a change of polarization. A second-order phase transition happens gradually without potential heat. In the crystal, the continuous lattice parameters and polarization are broken by an abrupt changing of temperature derivatives. When the materials transit from ferroelectric state to paraelectric state which has higher symmetry than former, the displacement of small atom arises dipole moments in the crystal. Aizu classified the phase transition into three types: "primitive", "complex" and others[8].

When a conductive material is placed on both surface of the ferroelectric forming short-circuit, with the change of temperature, an electric current is generated. This effect is known as pyroelectric effect that has been already used in the field of sensor and detector.

Another characteristic aspect of ferroelectricity is the polarization switching. Ferroelectrics have at least two nonzero polarization states which are thermodynamic stable[9]. The polarization states can be switched by applying an electric field, so-called E_c. This electric field is defined as a threshold for switching the residual polarization. The coercive field cannot be stronger than the breakdown field of the material. Not only the applied field but also temperature affects the ferroelectric switching process. The mechanism consists of three steps in most ferroelectrics. First, an inhomogeneous nucleation takes place at the surface of the electrodes followed by the needle-like domains growing parallel or antiparallel to the external field. Finally, the new domains grow laterally. The nucleation could be also the slowest step in other materials. In general, those three steps may occur simultaneously[10].

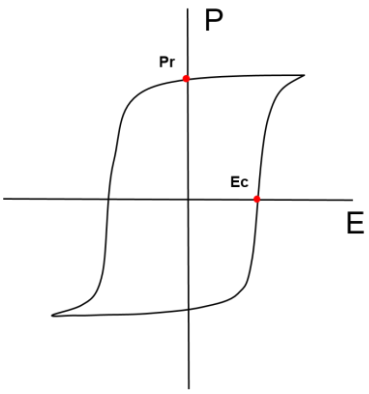

Figure 1. Polarization loop in the ferroelectrics.

The relationship between charge displacement and applied field is demonstrated in the hysteresis loop, shown in Figure 1. When the applied field is below the coercive field, it has no effect on ferroelectric polarization showing a linear result. As increasing the field to the coercive field, the materials begin to polarize. After reaching the highest value of polarization, the ferroelectrics stay at a saturated state. The coercive field is identified as the point at which the displacement changes sign on the x-axis. P_r is the intersecting value with y-axis when the field reduces to zero.

In terms of memory applications, one typically used device form for primary storage is the volatile memory. The stored data can be maintained only if the power is constant. In contrast, the non-volatile memory device retains information even after power-cycling. Ferroelectricity is an attractive property for the non-volatile memory device since the applied field is not essential to keep the storing function. Utilizing hysteresis loop we can contrive to integrate the polarization states with Boolean logical data type.

Thin-film ferroelectric capacitor is a simple memory device based on ferroelectricity. The device structure is shown in Figure 2a. Ferroelectric material is sandwiched between two electrodes. By applying an electric field, the direction of the internal polarization in ferroelectrics can be arrayed so that the information is preserved. However, upon the information is retrieved, a switching voltage pulse is applied that might change the polarization direction. Therefore, the ferroelectric capacitors are read-out destructive since they do not have resistive switching property. One promising solution is to develop a memory device that combines the ferroelectricity and electric conductivity. Figure 2b shows the hypothetical structure of the ferroelectric diode. Firstly, the devices perform desired properties of ferroelectrics such as non-volatility and bistability. Even when the power is turned off, the data are preserved in the ferroelectrics. Secondly, the semiconductor provides electrical conductivity and rectification. By applying a low bias, the device could be erased and read-out without destructing the information.

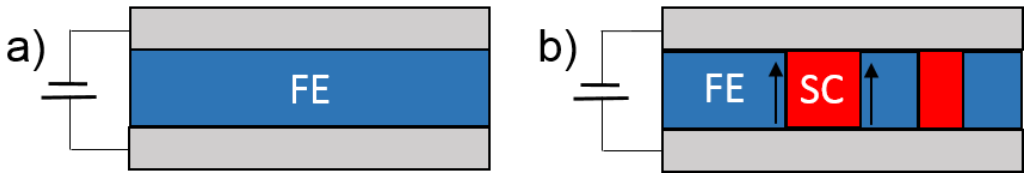

Figure 2. Device structure of a) ferroelectric capacitor. b) ferroelectric diode with the semiconductor (SC, red), ferroelectrics (FE, blue), and electrodes (grey). The black arrows indicate the current flow.

The bottleneck for this concept is to keep the advantages form both materials while reducing the high cost resulting from complex processing procedures. The organic materials provide a new idea in the field of large-area electronic applications, such as foldable displays, contactless identification and smart labels. Although they have lower mobility and degree of crystallinity compared with inorganic materials, they are low-cost, lightweight and provide numerous processing possibilities, e.g. solution-cast, ink-jet printing. They have good compatibility with multiple substrates and require low manufacturing temperature. By modifying their chemical structure, a variety of organic materials with tuned optoelectronic properties could be easily obtained. For small molecular organic semiconductor, the general processing approaches are sublimation and evaporation. Polymer semiconductors are deposited from solution by which a thin film over a large area is achieved[11].

1.2 Organic ferroelectrics

In recent decades, some small molecular organic ferroelectric materials have been synthesized successfully. Such low-molecular-mass material like thiourea, 2,2,6,6-tetramethyl-1-piperidinyloxy and 1,6-bis(2,4-dinitrophenoxy)-2,4-hexadiyne are not able to meet the demand for its low dielectric constant. New approaches have been developed according to the existing ferroelectric materials. As investigated in many polar molecules, the interaction between dipole usually leads to a cancellation of molecular dipoles. One available method is to take the analogy with ferroelectric oxides without polar ions into account. The spontaneous polarization in this mechanism originates from ionic displacement. Some unstable structures which can

generate spontaneous deformations in crystal lattice into a polar state are important for ferroelectricity. This mechanism usually takes place in the case when there is a balance between the electrostatic attractive force and the short-range repulsion force among the ions. Another mechanism is so-called proton transferring. In some organic systems containing hydrogen bonds (e.g., tricyclohexylmethanol) the bonding between H and O will break and the OH group then form a new connection around the C atom which reorients dipole[12].

According to the above-mentioned mechanisms, multi-components molecular system such as charge transfer donor-acceptor system and supramolecular system are more interested since the ferroelectric property has been enhanced[13]. For the charge transfer complex, the donor-acceptor chain could be polarized into a dipolar donor-acceptor dimer. Consequently, the polarity reverse between the donor-acceptor-donor and acceptor-donor-acceptor forms that accord with a displacement mechanism.

Owing to their widespread applications, synthetic polymers attract considerable attention. When piezoelectricity in polypeptides, poly(vinyl chloride) (PVC), poly(methyl methacrylate) (PMMA) and poly(vinylidene fluoride) (PVDF) was discovered, researches were then focused on the ferroelectric properties of polymers. PVDF (shown in Figure 3a) and its copolymers were regarded as the most widely used polymers in the field of electrics and biomedical engineering[14]. The current challenge is to develop polymeric materials with excellent pyroelectric, piezoelectric and ferroelectric properties.

PVDF was used as an insulator with large dielectric constant and as coating materials for its chemically stable property. After 1970 this polymer was considered to be a ferroelectric polymer whose ferroelectricity was hypothetically originated from either trapped space charges or molecular dipoles. The X-ray and IR results show the reoriented dipoles in crystal and hysteresis loop was also observed that increase its reliability[15].

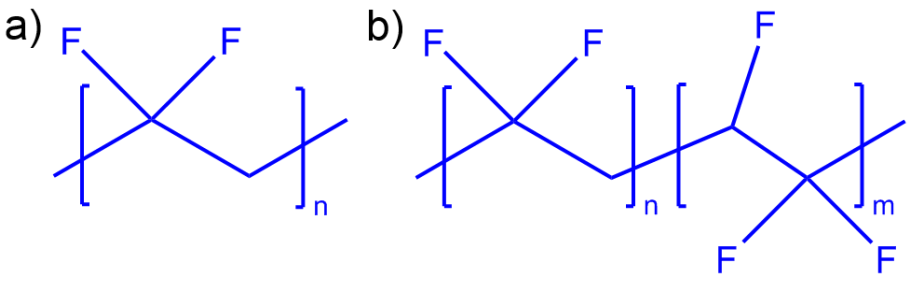

Figure 3. Chemical structure of a) PVDF. b) copolymer P(VDF-TrFE).

As mentioned before, the constitution of material should not be too bulky which inhibits polymer crystallization or results in large internal polarization cancellation. The polymer should also be chemically stable and will not form a cross-linked structure that is insoluble and infusible. Fluorocarbons are highly meeting the requirements since fluorine atom is small with Van der Waals radius of 135 pm. There is a strong polar bond between the carbon atom and fluorine atom. During the polymerization, the monomers are connected in $–CH_2\text{-}CF_2$ sequence in most

cases but connection defects such as $–CH_2-CH_2$ or $–CF_2-CF_2$ can be also found. Polymer chains are randomly coiled in the melt or in solution. By cooling down the melt chains without configuration defects are able to crystallize and organize a stable conformation. This procedure is achieved by rotating single bond to some position that has the minimal potential energy. Virtually the torsional angles arrange different from trans- and gauche conformations that are considered to be the two partial conformations.

In the family of polyfluoroethylene, when the polymers are rich in hydrogen, the conformation with the lowest potential energy is only preferred for its low rotational barriers. In contrast, if the polymers are rich in fluorine, bond rotation is impeded which restrict the conformation as well. PVDF with two hydrogen atoms and two fluorine atoms in every repeating unit is able to form different conformations since the hydrogen-rich part gives it flexibility. The fluorine-rich part then drives molecules to a stable conformation. Three conformations should be pointed out: all-trans, tg^-tg^+, $tttg^+tttg^-$. All-trans conformation has more polarity than the other two. When it comes to the polarity of crystal, chain packing is considered as another factor. According to diverse combinations of chain conformation and packing, four phases were obtained i.e.α-phase, β-phase, δ-phase and γ-phase[16].

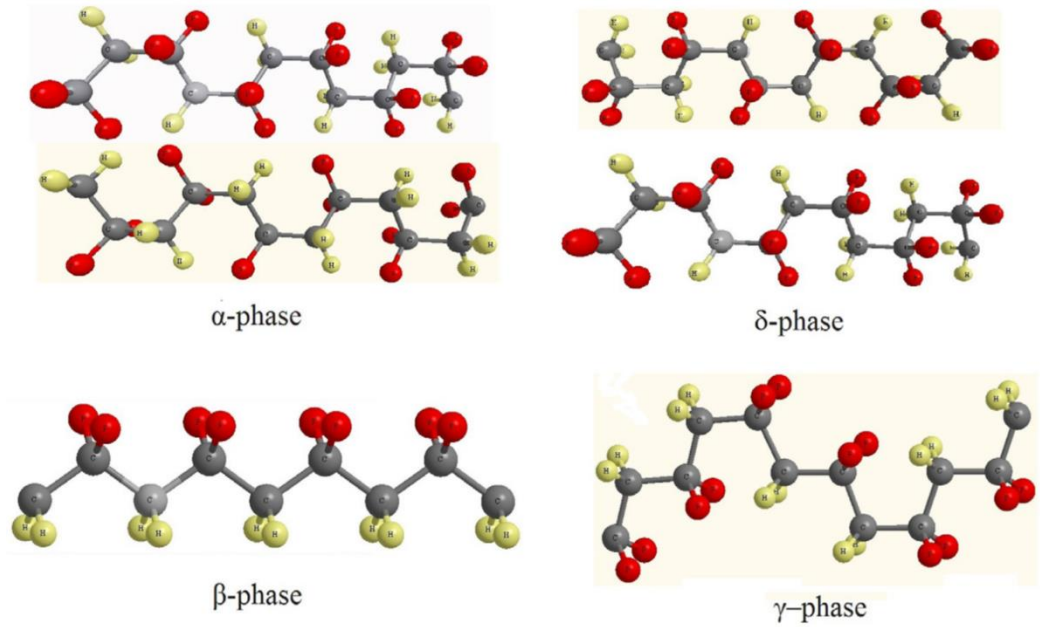

Figure 4. The α, β, δ and γ conformations of PVDF.

PVDF chains in α-phase are usually in tg^-tg^+ conformation. An antiparallel packing of two chains in the lattice gives rise to compensation of dipole moment and therefore α-PVDF are nonpolar. The α-phase is produced from polymer melt and is regarded as a stable polymorph. By applying a high electric field the polar δ-phase PVDF is obtained. The β-phase PVDF is known for its high polarity. In its unit cell, the all-trans conformational chains form parallel packing with dipoles in the same direction. At very high temperature the nonpolar α-phase could transfer into the polar γ-phase which has higher thermodynamic stability. However, the value of

spontaneous polarization of the β-phase PVDF is twice that of the δ-phase and γ-phase[17]. The four different conformations of PVDF was shown in Figure 4[18].

The melting temperature of PVDF ranges from 170 °C to 200 °C. The α-phase could be obtained by cooling down the melt and the crystal grows in a spherical structure. The highly polar β-PVDF is obtained from melt but by some special treatments[19]. Mechanical deformation at low temperature is a technique that forces the initial spherulites to alter in a well-oriented crystal that the molecules are in the same direction. Furthermore, applying a higher external electric field helps dipoles in the β-PVDF with the reorienting process.

Hasegawa[15]compared potential energy between the α and β phase. The results showed that it was not Coulombic interaction but Van der Waals interaction dominates the stability of crystalline phase. The β phase was just slightly less stable and indicated intermolecular dependence while the α phase was intramolecularly manipulated. Unlike traditional ferroelectrics such as $BaTiO_3$, whose spontaneous polarization results by Coulombic interaction, PVDF is considered as a special ferroelectric with its spontaneous polarization strongly influenced by Van der Waals interaction.

In the copolymers of vinylidene fluoride with trifluoroethylene (TrFE) or tetrafluoroethylene (TeFE), similar ferroelectricity has been also discovered. Figure 2b shows the chemical structure of copolymer P(VDF-TrFE).The idea of introducing TrFE and TeFE monomer came up in 1968 and the copolymers were synthesized in 1980 successfully. The copolymers contain 50-80% VDF monomeric unit. Due to the similar size of hydrogen and fluorine atoms, the distribution appears quite randomly along the polymer chain. The monomer with a larger ratio of fluorine atoms makes it difficult for chains to form tg^-tg^+ conformation. Instead, all-trans conformation is more preferred and thus the copolymer crystallizes in analogy to the β-phase PVDF. When the composition of VDF monomer is higher than 80%, the δ and γ phases would be favored. On the other, if copolymer contains less than 50% VDF, the ferroelectricity would largely be lost[15].

Another important aspect discovered in these copolymers is the Curie temperature. This phenomenon could not be seen in PVDF since its hypothetical Curie temperature is much higher than its melting point, as increasing the temperature beyond the Curie temperature transform into the nonpolar state. This process is reversible and can be explained in the molecular level as follows: owing to the introduced $g^\pm$ bound all-trans conformation changes into a disordered conformation containing $tg^\pm$ and tt sequences that leads to a random direction of dipoles.

When it comes into application field, vinylidene fluoride copolymers show its strengths. It was found that P(VDF-TrFE) polymer crystallizes much better than the PVDF polymer, especially after annealing treatment. Heating the copolymer between the Curie and melting temperature would sufficiently enhance the dimension of crystalline lamellar, accompanied with remnant polarization increment. PVDF has been mass produced in industrialization and is sold by many companies. Used as a coating layer for its stiffness, chemical resistance, wear resistance and

nonflammability is just one of the general applications. PVDF and its copolymer are easy to store and do not need special conservation. In recent twenty years, the nonvolatile memory devices based on PVDF and its copolymer have been developed that encourages the commercialization of organic ferroelectric memory technology.

1.3 Organic semiconductor

The other elemental part in a non-volatile memory device is the organic semiconductor. According to different conductivity, solid-state materials can be divided into three groups: conductor, semiconductor and insulator. The electrical conduction relies on electron motion through the transmission medium. The band gap between a fully electron-occupied band (valence band) and an unfilled band that has free electrons (conduction band) decides whether the electrons are able to be excited from low energetic valence band to higher energetic conduction band. For insulator, the band gap is too large that restricts electronic transition. On the other hand, conductor materials have overlapped valence and conduction band, therefore, there is no energy gap. Semiconductor presents both insulating and conducting properties. Figure 5 compares the band gap between insulator, semiconductors and conductors. At 0 K, it is an insulator whereas at room temperature it shows electrical conductivity. This is because of a small band gap between two bands (~1 eV). Semiconductor can be intrinsic such as Si and Ge or extrinsic so-called doped semiconductor. It is crucial for the chip industry, electronic devices, for instance, LEDs.

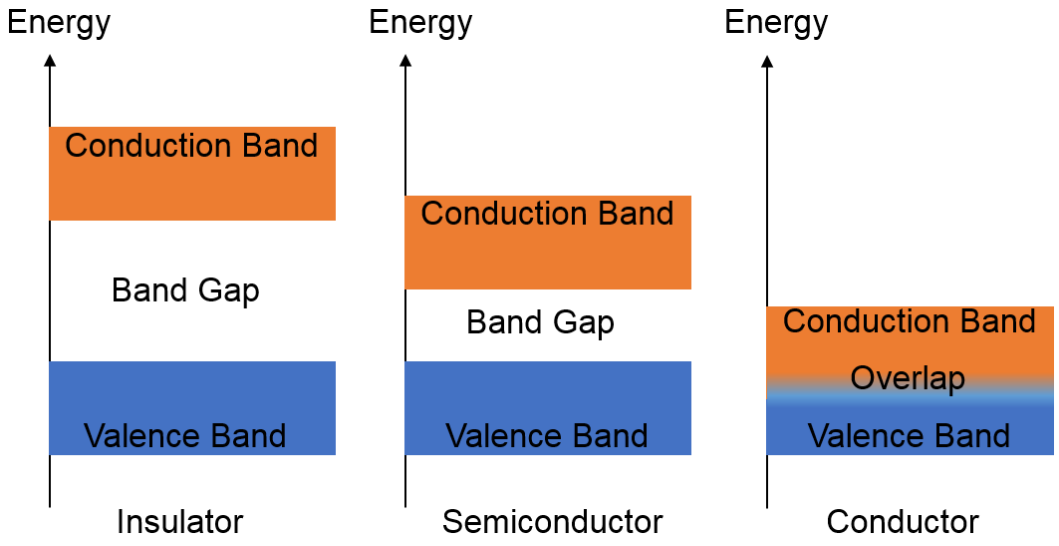

Figure 5. Band diagram of insulators, semiconductors and conductors.

The concept that semiconducting organic materials could be conductive was firstly introduced in 1948[13]. Halogen doped polyacetylene was revealed to be a semiconductor polymer by Shirakawa et al. in 1976. They synthesized both cis-isomer and trans-isomer films and found that the trans-isomer is more thermodynamically stable with higher conductivity. The organic semiconductors, i.e.

polymer semiconductor and small molecule semiconductor, have a conjugated system in common. The carbon atoms on the back bone are sp^2-hybridized which means a π electron is remained in the perpendicular p_z orbital per C atom (see Figure 6a). The π bond resulting from the overlap of neighboring p_z orbitals arises electron delocalization which allows charges to mobilize along the polymer chain (see Figure 6b). The π band is filled up with electrons whereas an empty π* band is left. The electron occupied π band is the highest occupied molecular orbital (HOMO) and the electron unoccupied π* band is the lowest unoccupied molecular orbital (LUMO). The energy difference between this two bands is the band gap, E_g that is manipulated by molecular structure.

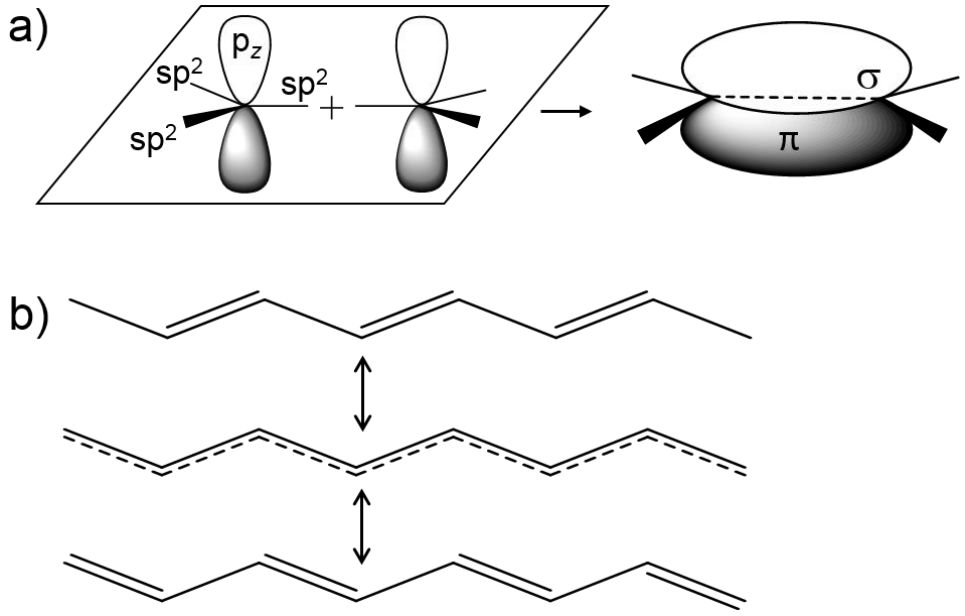

Figure 6. a) diagram of sp^2-hybridization. b) electron delocalization along the polymer chain.

The offset between the Femi energy level of metal and the molecular orbital energy level defines the interface energy barrier and thus three types of electron contact injecting into semiconductor are explicated: Ohmic, neutral and injection-limited contacts. However, the electron injection behaves somewhat differently in reality. The current reaches its maximum in the case when the charge is saturated depending on electrostatics. This observation is called space charge limited current. Under this circumstances, current density J is related to the applied voltage (V) and film thickness (L) and follows the Mott-Gurney equation:

$$J = \frac{9}{8}\varepsilon\varepsilon_0\mu\frac{V^2}{L^3} \quad (1)$$

ε: dielectric constant of the polymer semiconductor

ε_0: the vacuum permittivity

μ: charge carrier mobility.

At low voltage, the current measured in conjugated polymers is lower and this is defined as diffusion regime. The reason for such a different experimental phenomenon is that the polymer chains are strongly disordered. The disordered polymers have interfering impacts on energy band formation and usually exhibit broadening HOMO- and LUMO levels distribution. It was revealed that if the contact barrier is larger than 0.25~0.3 eV, the current which is supplied by the contact is small. Thus, it is considered to be injection limited. If the contact barrier is around 0.25~0.3 eV, there is built-up charge effect. If the barrier is lower than 0.25~0.3 eV, a space charge limited current would be expected[20].

The organic semiconductors have higher degree of disorder. Unlike well-crystallized inorganic materials, it gives rise to comparative differences in thermodynamic and mechanical properties including decreased melting point and hardness. In addition, the more significant impact for semiconductor is the weaker electronic delocalization among adjacent chains that directly influence charge transport.

The charge carrier transport mechanism is different for pure crystalline molecules and amorphous organic solid. For organic semiconductor, the mechanism is described between those two cases. Band transport applies to higher order organic crystals at low temperatures. With temperature decreasing, the behavior of charge with temperature is shown as follows:

$\mu \propto T^{-n}$, n =1…3

The weak delocalization in semiconductor materials results in a small bandwidth displaying a few kT at room temperature. Thus the mobility ranges just from 1 to 10 cm^2/Vs at room temperature. In addition, the electron traps effect deviates the temperature dependent behavior remarkably.

When it comes to amorphous organic solids such as polymer semiconductors, hopping transport is observed that gives much smaller mobility of 10^{-3} cm^2/Vs. The charge carrier mobility μ relies not only on temperature (T) but on the applied field as well following exponential behavior with activation energies ΔE between 0.4 and 0.5 eV[21]:

$$\mu(F,T) \propto \exp\left(-\frac{\Delta E}{kT}\right)\exp\left(-\frac{\beta\sqrt{F}}{kT}\right) \quad (2)$$

F: electric field

k: Boltzmann constant

β: model-dependent constant

If parameter σ is introduced which represents the width of the Gaussian distribution of the density of states, the relationship could be alternatively expressed as[22]:

$$\mu(F,T) \propto \exp\left(-\left[\frac{2\sigma}{3kT}\right]^2\right)\exp\left\{C\left(\left[\frac{\sigma}{kT}\right]^2 - \Sigma^2\right)\sqrt{F}\right\} \quad (3)$$

Σ: width of variable distribution of the density of states.

C: concentration dependent parameter

When the material is used in an electric circuit, the current density is often calculated from carrier density n, the charge carrier mobility μ and electric field F. Since the carrier density and carrier mobility are both related to the electric field, the current density in organic semiconductor shows non-linear behavior to the applied field. The preparation process and operation environment play an important role on structure regularity and purity in the organic semiconductor which determines the charge carrier mobility (in crystals 1 to 10 cm^2/Vs and in amorphous solids lower than 10-3 cm^2/Vs). As for the charge carrier density n, it is given by energy gap E_g and the density of molecules in an organic semiconductor N:

$$n = N \exp(-\frac{E_g}{2kT}) \quad (4)$$

Comparing with inorganic semiconductor, the conductivity of the intrinsic organic semiconductor is many orders of magnitude lower. By a number of approaches to enhance the carrier density such as doping, carrier injection and carrier photogeneration, the performance has been improved.

1.4 Phase separation in polymer blends

Apart from copolymer synthesis, mixing at least two polymers enables to combine different properties. The resulting product is called polymer blends and usually shows improved performances. Polymer blends could be classified into immiscible polymer blends, partially miscible polymer blends and miscible polymer blends.

Immiscible polymer blends are a mixture of two polymers at physical level performing as the phase separation. The morphology depends strongly on the components of a mixture. An example of phase separation morphology of immiscible binary blends is shown in Figure 7 The minority component B (in blue) forms spherical shape and randomly distributes in the majority component A (in red). As the volume of component B increasing, the system presents bicontinuous phase separation. Keeping increasing the component B, a reversed phase separation is obtained, in which case component A is surrounded by the matrix B. The dimension of those spherical domains is usually in micrometer range. For immiscible polymer blends, one prominent character is that the glass transition temperature of respective components could be observed.

Partially miscible polymer blends exhibit macroscopically homogeneous or heterogeneous influenced by the temperature, pressure and composition. Miscible polymer blends show only single phase and unitary glass transition temperature which is between the glass transition temperatures of two pure components.

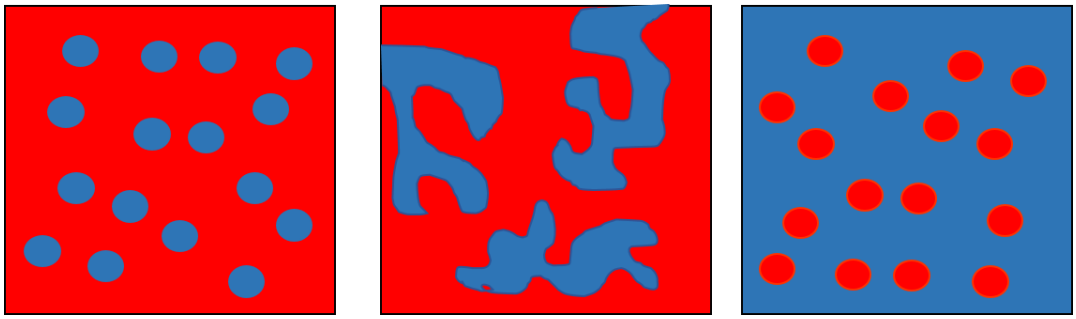

Figure 7. Immiscible polymer blends as an example for morphology.

The thermodynamic process of mixing can be described by Gibbs free energy:

$$\Delta g_{mix} = \Delta h_{mix} - T\Delta s_{mix} \quad (5)$$

Δh_{mix} is the enthalpy change of mixing, Δs_{mix} is the entropy change of mixing and T is temperature. When the change of Gibbs free energy is negative, the mixing process is spontaneous. Normally the value of entropic change during mixing is positive because the randomness in the system is increased. In statistical thermodynamic, this can be rewritten as:

$$\frac{\Delta g_{mix}}{k_b T} = \frac{\emptyset_A}{N_A} \ln \emptyset_A + \frac{\emptyset_B}{N_B} \ln \emptyset_B + \chi \emptyset_A \emptyset_B \quad (6)$$

$$\emptyset_B = 1 - \emptyset_A \quad (7)$$

also known as Flory–Huggins equation[23][24] for the binary system. k_b is Boltzmann constant, T is temperature, $\emptyset$ and N are volume fraction and degree of polymerization of each component respectively.

The term χ is the Flory-Huggins parameter. It is dimensionless and determines the interaction between different components in the mixture which can be obtained from:

$$\chi = \frac{Z}{k_b T}\left(w_{12} - \frac{w_{11}+w_{22}}{2}\right) \quad (8)$$

z: the coordination number

w_{12}: solvent-monomer interaction

w_{11}: solvent-solvent interaction

w_{22}: monomer-monomer interaction

In the Flory-Huggins equation, the entropy term is significantly related to the chain length. In comparison with small molecules, the increasing degree of polymerization leads to the decrease favorable entropy of mixing which makes it difficult to mix polymer species.

Empirically, the Flory–Huggins parameter can also be written as[25]:

$$\chi(T) = A + \frac{B}{T} \tag{9}$$

It simplifies the relationship between interaction parameter and temperature. The term A and B/T are considered to be the entropic and enthalpic contributions to the χ parameter.

Since χ parameter has temperature dependence, phase diagrams, showing temperature T as the function of volume fraction $\emptyset$, could be represented in two classes. In an endothermal polymer mixture the entropic contribution to local Gibbs free energy is marginal and the B parameter a positive value. As temperature decreases, the χ parameter is increased. This transition temperature at which the single-phase state changes into the two-phase state is called the upper critical dissolution temperature (UCST). For an exothermal polymer mixture, with a negative B parameter, the one-phase region appears at low temperature and the components become immiscible with increased temperature. In this case, the transition temperature is called the lower critical solution temperature (LCST).

Figure 8a,b show the typical phase diagrams of binary UCST and LCST systems. In the phase diagram, the boundary between the single-phase region and the coexistence region is binodal curve. It is defined by the composition $\emptyset_A$ and $\emptyset_A$, coexisting at equilibrium with minimum free energy in the miscibility gap. Furthermore, there is also a limit that divides the phase-separation region into metastable- and unstable region. This limit is called spinodal curve, on which the second derivation of Gibbs free energy is zero. The point where binodal and spinodal meet is the critical point.

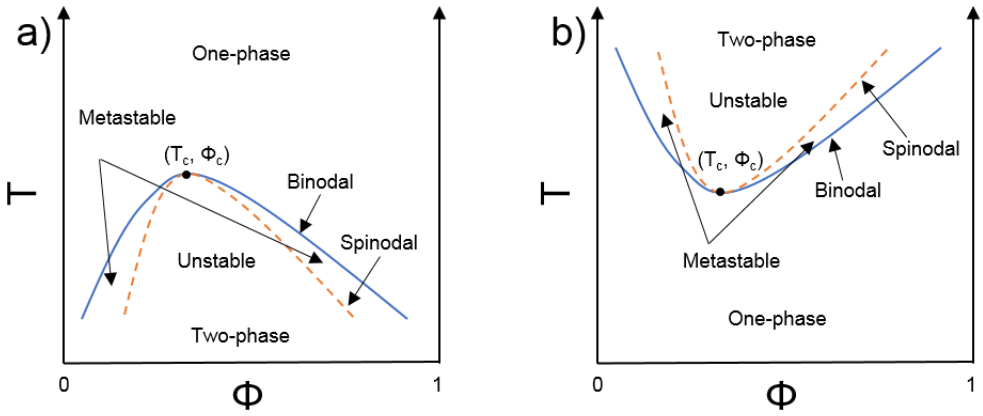

Figure 8. Phase diagram of a non-isothermal binary system: a)UCST b)LCST. The binodal curve is pointed with blue solid line and the spinodal curve is pointed with the orange dash line.

Spinodal decomposition and nucleation and growth are the two basic phase separation mechanisms. The schematic diagram is seen in Figure 9. Whether phase separation occurs via nucleation and growth (metastable demixing) or spinodal decomposition (unstable demixing), that influences the structure evolution.

The sudden temperature jump can bring spontaneous phase separation. The compositions in the two phases are then defined by the values on the coexistence curve at that temperature. This spontaneous phase separation is spinodal decomposition that takes places when the mixture is globally unstable. Even small local concentration fluctuation lowers the free energy, initiating a spontaneous phase separation. In Figure 9b, the flow direction of the component goes towards a higher concentration implying that the amplitude of concentration fluctuation grows continuously.

On the other hand, the metastable homogeneous state locating between the binodal and spinodal curves is locally stable against small concentration fluctuations. The phase separation is only initiated by a larger nucleation to achieve equilibrium. Once it occurs it can expand in size. This process is nucleation and growth. Figure 9a indicates that the flow goes to the region where concentration is decreased[25].

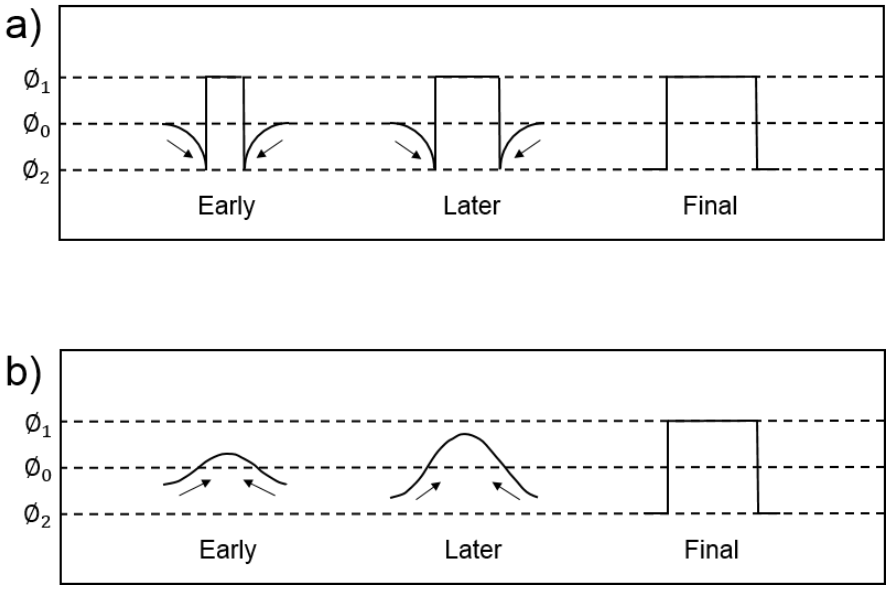

Figure 9. The mechanism of phase separation: a) nucleation and growth. b) spinodal decomposition.

In many organic electronic devices, at least one of the essential parts contains a blends layer processed by solvent-casting. The Flory-Huggins model of such polymer-polymer-solvent ternary system can be written as[26]

$$\frac{\Delta g_{mix}}{k_b T} = \frac{\emptyset_A}{N_A}\ln \emptyset_A + \frac{\emptyset_B}{N_B}\ln\emptyset_B + \emptyset_s \ln\emptyset_s + \chi_{AB}\emptyset_A\emptyset_B + \chi_{AS}\emptyset_A\emptyset_S + \chi_{BS}\emptyset_B\emptyset_S \quad (10)$$

$$\emptyset_A + \emptyset_B + \emptyset_S = 1 \quad (11)$$

where $\emptyset_S$ is the volume fraction of solvent, χ_{AB}, χ_{AS} and χ_{BS} are the Flory-Huggins interaction between two polymers and polymer-solvent. The size of solvent is set to unity.

During fast solvent evaporation, the dissolved polymer components spontaneously demix. The blend is quenched from single-region into unstable region of the ternary

phase diagram. The final morphology strongly relies on the solvent-quenching stage after which the increased viscosity somehow block the mass transport and therefore, the molecular mobility is low[28]. Compared to binary mixture, the ternary system shows an isothermal phase diagram. (see Figure 10)

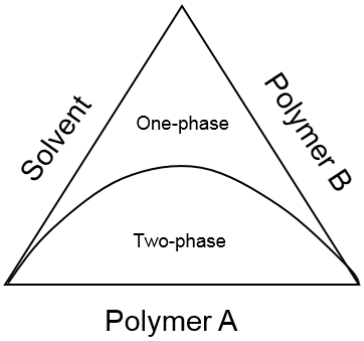

Figure 10. Phase diagram of a ternary system.

In recent years, the morphology of the solution-casting blends layer based on ferroelectric and semiconducting polymers have been investigated. The ferroelectric polymer P(VDF-TrFE) form a matrix in which the organic semiconductors such as poly(9'9-dioctyl-fluorene)(PFO), regio-irregular poly(3-hexylthiophene)(rir-P3HT) and poly[(9,9-dioctylfluorenyl-2,7-diyl)-alt-co-(1,4-benzo-{2,1',3}- thiadiazole)] (F8PT) are dispersed [2][27][29][30][31]. Combining ternary diffuse interface theory and extended Flory-Huggins theory of the homogeneous free energy of mixing, the phase separation is described by spinodal decomposition. In the initial stage, the formation and growth of the semiconductor domains are induced by the small density fluctuation. In a later stage, the domain is coarsening that reduces the total interfacial area. The number of domains per unit area decreases with time. As a result, the driving force for further coarsening decreases. Finally, as long as the mobility of blend components keeps high, the system will reach equilibrium. However, in practice, the components are vitrified by the ongoing solvent evaporation far away from thermodynamic stability[31].

1.5 Non-volatile memory diodes

The concept of memory diode is based on non-volatile resistive switches using phase-separated blends of a semiconductor polymer and a ferroelectric polymer. The bistable diodes possess a tunable injection barrier which could be modulated by the polarization field of ferroelectrics at the semiconductor-electrode contact. The semiconductor provides signals to demonstrate whether the diode is programmed into a high resistance OFF-state or a high conductance ON-state.

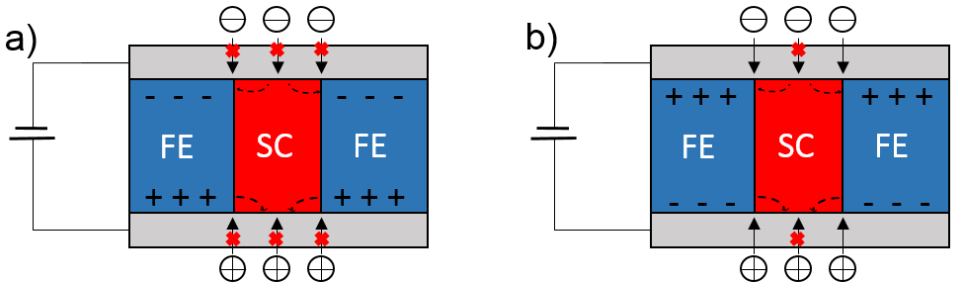

Figure 11. Cross-sectional schematics of the memory device, with the semiconductor (SC, red), ferroelectrics (FE, blue), and electrodes (grey). a) The device is poled in the OFF-state. b) The device is poled in the ON-state. The charge compensation in the interface of ferroelectric and semiconductor interface (black arrows) and the stray field (dashed black arrows) are depicted respectively.

The electrical characteristics and morphology of the active layers of such devices have been investigated. Non-volatile switching is attributed to the electric field responding bistable polarization of ferroelectrics. Conductivity is from semiconductor polymer. Figure 11 shows the tentative operation mechanism. The ferroelectric polymer is completely insulating, therefore, the semiconductor is the only medium that allows current flow through. One electrode metal is chosen to yield a large injection barrier deliberately. This large injection barrier prohibits charge injecting process and leads to low current. However, the injection barrier is tunable as long as the polarization direction of ferroelectric is changed. When ferroelectric is poled along the direction of the external electric field, the injection barrier is increased and current is suppressed appearing an OFF-state (Figure 11a). In contrast, when ferroelectric is poled inversely, with opposite polarization direction to the probing bias, the negative polarization is compensated for by accumulation of holes in the semiconductor domains. As a consequence, the band is bent strongly, which lowers the injection barrier. The current then becomes space-charge limited and the diode is in ON-state (Figure 11b).

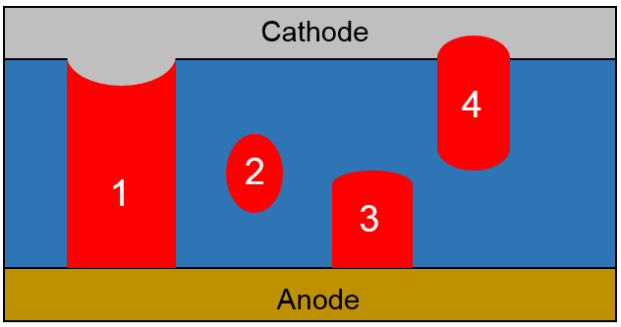

Figure 12. Cross-sectional schematic of complete phase-separation polymer blends film between the top electrode (grey) and the bottom electrode (yellow) in practice. The ferroelectric matrix and semiconductor domains are indicated in blue and red, respectively.

In practice, many factors contribute to the final phase geometry such as the interfacial force and evaporation time. Therefore, not all the semiconductor domains form the ideal morphology as shown in Figure 11. Figure 12 depicts different types of semiconductor domain morphology in ferroelectric matrix in non-ideal case[33]. The “type 1” are the domains that percolate through the whole film, bringing from the top electrode to bottom electrode. The “type 2” domains are fully embedded with

neither contact to top electrode nor bottom electrode. The size of this type is significantly smaller than film thickness. The “type 3” domains are located on the bottom electrode but are buried in the matrix whereas the “type 4” domains float on the ferroelectric matrix and only have a connection with the top electrode. The “type 1” is the electrically efficient one that allows the current to flow through the device.

So far, organic semiconductors such as PFO, P3HT and F8BT (see Figure 13) have been investigated in the field of non-volatile ferroelectric memory device. Blending these polymers with ferroelectric polymer, all systems demonstrate a complete phase separation that meets one of the requirements for a working device. The morphology plays a crucial role in device performance The side chains which can be linear or branched are joined with rigid carbon backbone. They directly affect the solubility of polymers. Besides, film construction, polymer conformation, crystalline property, backbone torsion and special electron displacement are also influenced by side chains. It has been reported that the steric constraint between adjacent aromatic units gives rise to intramolecular interaction. This kind of interplay is the main reason for backbone torsion and electronic properties are consequently impaired. The steric influence between two hydrogen atoms in the biphenyl units extremely inhibit coplanarity of benzene rings while in bithiophene structure it is much easier to reach coplanar.

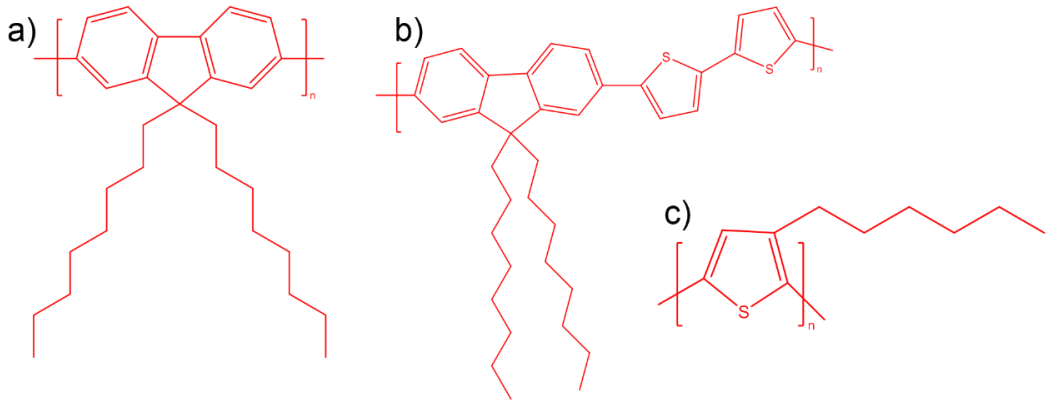

Figure 13. Chemical structure of a) PFO, b) F8BT and c) P3HT.

2 Scope

PCDTBT polymer works as a p-type semiconductor material in the active layer of organic photovoltaic devices. This semiconductor material with low band gap exhibits remarkable thermal stability. One particular bulk heterojunction solar cells combined PCDTBT with fullerene derivative achieved 10% higher internal quantum efficiency and a lifetime for up to 7 years compared with previous reports[34][35].

Due to its low-lying HOMO level, PCDTBT is also available as an acceptor for those strong donor polymer materials forming conjugated donor-acceptor block copolymers, which are great attractions for organic optoelectronics[36]. The morphology on nanoscale of donor-acceptor networks is the key for device performance. Some block copolymers systems such as PCDTBT/P3HT and PCDTBT/PCBM utilized as organic solar cell has been reported[37]. In such cases, microphase separation is essential to achieve charge separation, transportation and reduce charge recombination. By side chain engineering, the Flory-Huggins interaction parameter can be adjusted and furthermore influences the compatibility of polymer segments.

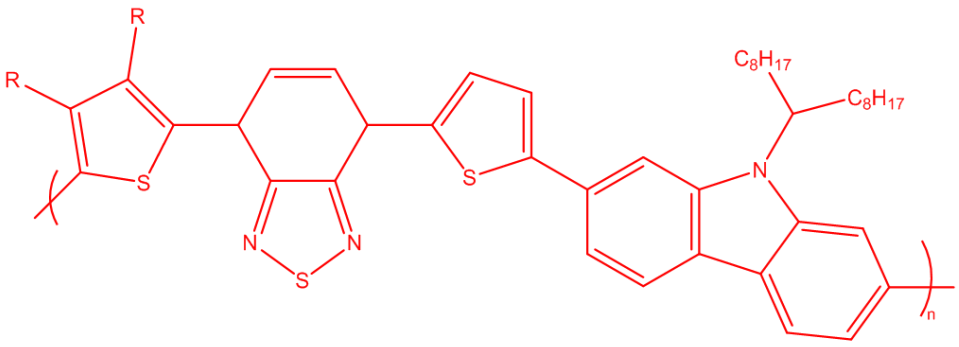

Hexyl-PCDTBT R= $-C_6H_{13}$
SF-PCDTBT R= $-C_4H_8C_4F_9$

Figure 14. Chemical structure of PCDTBT polymers.

Replacing the hydrogen atoms of the thiophene rings by hexyl alkyl side chains or semifluorinated alkyl side chains respectively, the results are somehow divergent. For solar cell devices, the hexyl alkyl side chains give rise to increasing backbone torsion that enhances electroluminescence and photoluminescence. Both side chains increase dissimilarity of segments, however, the block copolymers with semifluorinated side chains are more prone to phase separate. The device efficiency, therefore, exhibits 1% larger power conversion than the one with hexyl alkyl side chains.

While considerable attention has been drawn in the optoelectronic field, this attempt is much less investigated among organic memory devices. Here, we blend non-fluorinated and partially fluorinated PCDTBT materials (Figure 14) synthesized in the group of Prof. Michael Sommer (University of Chemnitz) with the ferroelectric polymer P(VDF-TrFE). We aim to progress the insight into how the phase separated morphology couples with device performance. In this sense, we anticipate the

fluorinated PCDTBT to have an improved compatibility (lower Flory-Huggins interaction parameter) with the ferroelectric polymer, possibly leading to a very different phase morphology and composition than typically observed. Microscopic technique will be used to study the influence of fluorination of the alkyl side chains of the semiconductor on the phase behavior and morphology. Thin-film memory devices will be fabricated and electrically characterized to identify the relation between the miscibility and device performance.

3 Experimental Section

3.1 polymer blends solution preparation

The ferroelectric copolymer P(VDF-TrFE) (M_w=400 kDa,75%-25%) was purchased from Solvay. The polymer semiconductor PFO(M_w=264 kDa, D=2.87) was synthesized according to Yamamoto polymerization. Hexyl-PCDTBT(M_w=78 kDa, D=2.05) and SF-PCDTBT(M_w=58 kDa, D=1.81) were supplied by AK Sommer from Chemnitz University of Technology. The blends solutions in degassed THF(Sigma-Aldrich) was prepared by co-dissolving semiconductor polymer and P(VDF-TrFE), yielding a blends weight ratio of 9:1 P(VDF-TrFE)/PFO, 5:1,9:1, 12:1 or 18:1 P(VDF-TrFE)/SF-PCDTBT and 4:1,9:1 P(VDF-TrFE)/Hexyl-PCDTBT. Solutions of 20 mg/mL PFO/P(VDF-TrFE), of 26~28 mg/mL PFO/P(VDF-TrFE) and PCDTBT polymer/P(VDF-TrFE) were designed. A hot gun was used to heat the P(VDF-TrFE)/PFO solution intermittently followed by stirring the solution at 45 °C for 5 minutes. P(VDF-TrFE)/SF-PCDTBT and P(VDF-TrFE)/Hexyl-PCDTBT solutions were stirred at 55 °C for 15 minutes. Clear solutions were obtained after cooling and were filtered with 1 µm PTFE filters. The differences between each set are detailed in Table 1.

Table 1. Overview of all experimental conditions.

Semiconductor	Weight ratio	Concentration	Substrate
PFO	1:9	20	Glass
PFO	1:9	20	Au deposited glass
PFO	1:9	26~28	Au deposited glass
SF-PCDTBT	1:5	26~28	Au deposited glass
SF-PCDTBT	1:9	26~28	Au deposited glass
SF-PCDTBT	1:12	26~28	Au deposited glass
SF-PCDTBT	1:18	26~28	Au deposited glass
Hexyl-PCDTBT	1:4	26~28	Au deposited glass
Hexyl-PCDTBT	1:9	26~28	Au deposited glass

3.2 polymer blends film preparation

Glass slides were cleaned in soap, sonicated in acetone and propanol and dried with nitrogen gun. Two sets of substrates were prepared. Set 1 on the clean glass substrate. Set 2 on the metal-coated glass substrate. The polymer blends solutions were spin coated onto substrates in a nitrogen-filled glove box (Figure 15). The spin rotation speed was 1000 rpm. The samples were then annealed in a vacuum oven at 142 °C for 2 h in order to increase the crystallinity of ferroelectric polymer P(VDF-TrFE). For samples of set 2, 50 nm of gold with 1 nm of chromium layer were deposited through shadow masks by the organic evaporator.

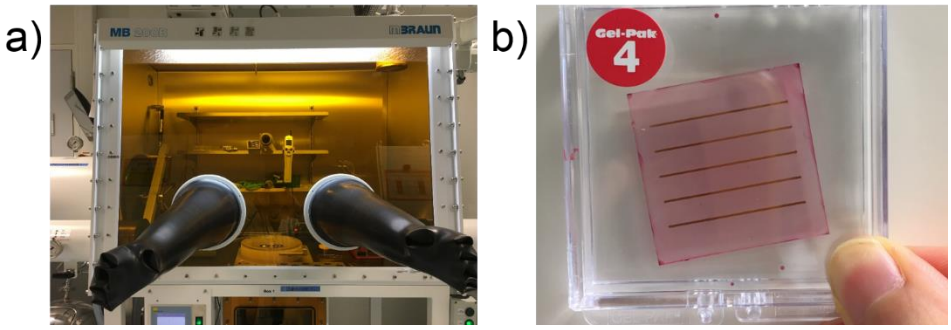

Figure 15. a) Picture of spin-coater in Glove Box and b) SF-PCDTBT/P(VDF-TrFE) blends film on Au deposited glass substrate.

3.3 selective dissolution

For selective dissolving technique, DMSO and toluene were used to selectively dissolve the ferroelectric polymer P(VDF-TrFE) and semiconductor. DMSO was purchased from Sigma-Aldrich. Toluene was purchased from Fischer Chemical. Both solvents were degassed. The polymer blends samples were placed on spin-coater in a nitrogen-filled glove box. A certain amount of solvent dropped on polymer blends surface, followed by standing the sample for two minutes. After a defined spin coating procedure, the solvent was flash-evaporated.

3.4 memory devices fabrication

For memory devices, 50 nm gold was deposited on the clean glass substrate with 1 nm Cr adhesion layer as the bottom electrode. After spin-coating the blends film, 100 nm Al was evaporated on top of the film via a shadow mask. For PFO/P(VDF-TrFE) solution of 20 mg/mL, an extra PEDOT: PSS were added between the polymer blends film and top electrode to avoid a high leakage current in case of a thin blends layer. Since PEDOT: PSS is water soluble, a few drops of Zonyl®FSO-100 (DuPont) for surface activation were mixed with PEDOT: PSS before spin coating. The dimension of the memory device is 400 µm × 400 µm. The layout of finished devices is shown in Figure 16.

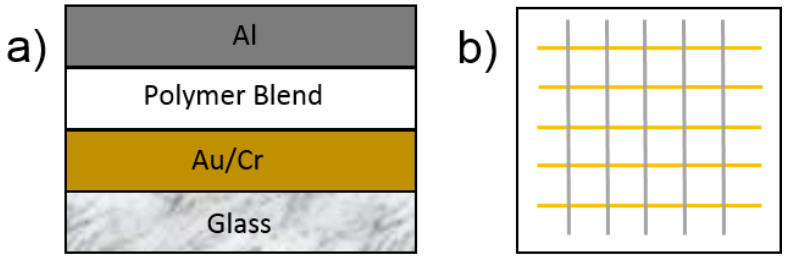

Figure 16. a) Cross-sectional schematic of memory device. b) Top view of memory device.

The devices for electroluminescence study were fabricated with different masks. As bottom electrode, a 20 nm gold layer with 1 nm Cr adhesion layer was used

obtaining a semitransparent anode. Top electrode was a 15 nm barium layer capped with 100 nm aluminum that deposited trough OLED mask.

3.5 Measurement and Characterization

3.5.1 Film thickness

A DEKTAK profilometer was used to measure the film thickness. This instrument equips with a diamond stylus. During the measurement, stylus drops vertically onto the sample surface and then moves across the sample in the lateral direction for a set distance and contact force in either valley or hill mode. The accuracy of vertically features ranges from 10 nm to 65 µm with 0.5 nm resolution. With a video camera, stylus is able to be placed manually and the system is programmed for scan speed and scan length. The film thickness of PFO/P(VDF-TrFE) of 20 mg/mL concentration was 180±5 nm. The solution of higher concentration i.e.26~28 mg/mL gives a thicker layer thickness of 300±5 nm. For PCDTBT polymer, SFPCDTBT polymer blends solution gave a layer thickness of 250±5 nm.

3.5.2 AFM

Surface topography of polymer blends film was investigated with AFM (Veeco Dimension 3100, Veeco Digital Instruments by Bruker). The morphology was performed using a sharp scanning probe in tapping mode. During measurement, a laser beam is reflected from a cantilever and detected in the electronic feedback loop. The topographical results of annealed blends film and selective dissolved film were depicted in both height and phase imaging modes.

3.5.3 SEM

A low-voltage and high-resolution SEM from Zeiss(Leo Gemini 1530) is used to investigate the morphology of polymer blends film. SEM is one of electron microscope using either secondary electrons or backscattered electrons that images sample surface by surface scanning. The accelerate voltage could be varied between 100 V and 30 kV with a resolution about 1 nm. Toluene treated and untreated SF-PCDTBT/P(VDF-TrFE) as well as Hexyl-PCDTBT/P(VDF-TrFE) polymer blends substrates were scanned.

3.5.4 Electrical properties

The current-voltage measurement and retention time measurement of devices were carried on in vacuum (~10^{-6}) and dark environment with HP 4155B semiconductor parameter analyzer. The tests proceed under the ambient temperature and in dark.

The devices are sensitive to oxygen and light. Therefore they should be stored in a closed container in the nitrogen-filled glove box. For current-voltage measurement, bias was applied on the gold electrode and the Al electrode contacted to ground. The voltage swept from negative bias to positive bias then swept back to negative bias again forming an I-V loop. To switch the devices, voltage pluses that larger than coercive bias were applied. The I-V sweep was sequentially performed for voltages quite lower than coercive voltage.

In retention time measuring, the devices were first switched to high conductive ON-state and measured over a period of time. Subsequently, devices were switched to low conductive OFF-state and measured the OFF-current as the same way.

3.5.5 Electroluminescence

Devices were fabricated by the same method as mentioned in memory devices fabrication part with the OLED mask (Figure 17). The active area of each device amounted to 1 mm ×1 mm and devices were measured in nitrogen protect environment. The electroluminescence was measured with a source meter Keithley 2400.

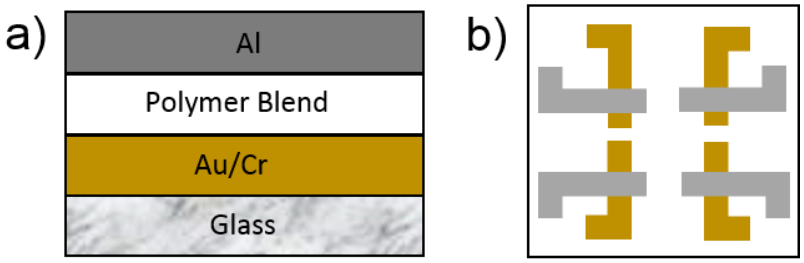

Figure 17. a) Cross-sectional schematic of electroluminescence device. b) Top view of electroluminescence device.

4 Results and Discussion

4.1 Morphological Characterization

The solution-cast and annealed polymer blends films with different blends ratio semiconductor/ferroelectric according to the previous work[29] were characterized with various microscopic techniques.

AFM measurement was conducted to investigate the phase separation and microstructure. The probe was scanned across at the blend/air interface revealing the morphology of blends films spin-coated on glass and gold substrate.

4.1.1 PFO/P(VDF-TrFE) blend

Figure 18 shows AFM height and phase image of the PFO/P(VDF-TrFE) blends of 20 mg/mL after annealing on glass substrate. Phase image presents circular shape PFO domains are embedded in the continuous P(VDF-TrFE) matrix randomly. From height image some PFO domains (brighter dots) formed a convex shape that protrudes from the film, resulting in a rough surface. The size of PFO domains is around 250 nm.

During solution casting, the polymer separation gave virtually discrete domains since there is a strong repulsion between those two components. The surface roughness likely results from height difference between the phase domains as a consequence of solvent partitioning. If the surface roughness is comparable to the layer thickness, the electrical shorts will happen to a large extent when the devices are fabricated.

The crystallinity of P(VDF-TrFE) was enhanced by annealing procedure which hardly influences the microstructure of the amorphous polymer PFO. Crystalline β-phase P(VDF-TrFE) presents a rice-like shape. The ratio of area occupied by the two polymers is also in the line with experimental section (1:5 volume ratio as $\rho_{P(VDF-TrFE)}$: $\rho_{PFO} \sim 1.8$).

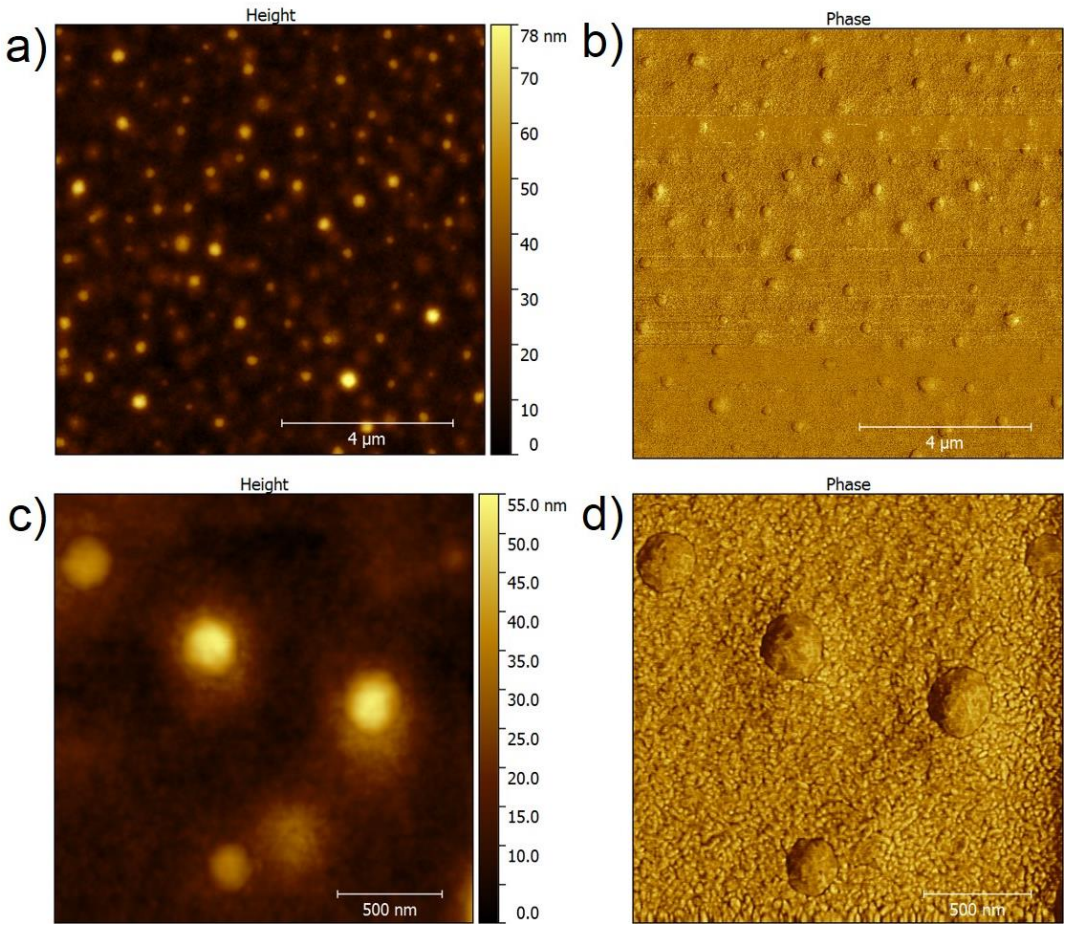

Figure 18. AFM images of a film of PFO/P(VDF-TrFE) blends (1:9 w/w ratio, 20 mg/mL) on glass substrate after annealing at 140 °C. a) c) AFM height image. b) d) phase images at different scales.

A similar morphology of polymer blends could be found on the substrate deposited with gold. Figure 19 shows the surface morphology of PFO/P(VDF-TrFE) blends on Au. Two different concentration values i.e. 20 mg/mL and 26~28 mg/mL are studied. DEKTAK profilometer indicates film thickness of 180±5 nm and 300 ±5 nm. In both cases, disk-shape minor component PFO domains (brighter part in phase image) are embedded in the ferroelectric matrix with a surface roughness comparable to film thickness. The unambiguous sphere-shaped domains are the evidence of minimizing surface tension between two components during phase separation. Two types of PFO domains are observed on Au. One with average diameter of 470 nm has a concave top. Another with larger average diameter of 700 nm has a convex top. The domain size on Au is significantly larger than on glass substrate even with the same concentration. However, increasing the concentration of polymer blends solution only has a negligible impact on domain size and domain distribution.

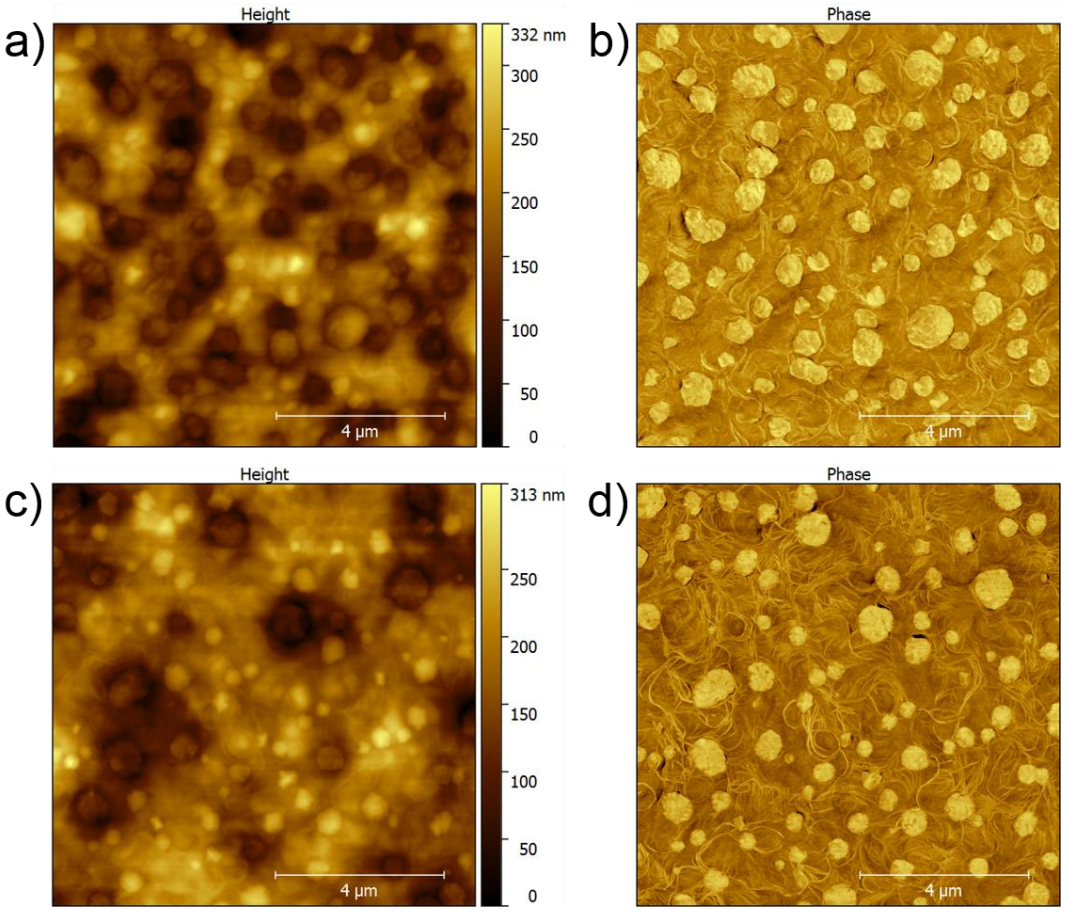

Figure 19. a) b) AFM height and phase images of an annealed film of PFO/P(VDF-TrFE) blends (1:9 w/w ratio, 20 mg/mL) on gold. c) d) AFM height and phase images of an annealed film of PFO/P(VDF-TrFE) blends (1:9 w/w ratio, 26.7 mg/mL) on gold.

This morphological observation is agreement with SEM images obtained on the same film, shown in Figure 20. The images present a clear contrast: separate circular dark gray domains are randomly distributed in the gray needle-like matrix. The domain is of the order several hundred nanometers and seems amorphous. Therefore, annealing treatment only enhanced β-phase in ferroelectrics and barely influenced the microstructure of the phase separated blend.

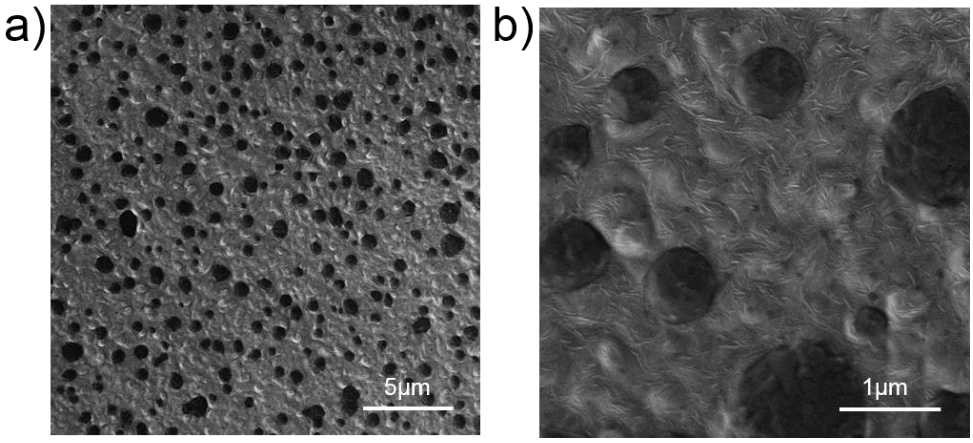

Figure 20. a) b) SEM images of a film of PFO/P(VDF-TrFE) blends (1:9 w/w ratio, 27 mg/mL) on gold after annealing at 140 °C.

In order to obtain the statistical data, the SEM images were imported in image processing ImageJ for quantitative analyzing. Figure 21 indicates the PFO domain diameter distribution functions, i.e., cumulative distribution function and probability distribution function in the 1:9 ratio blends film. The bell-shaped distribution functions interpret that the PFO domains with a diameter between 550 nm to 600 nm are the most. The data in the histogram are right-skewed which shows most of the domain diameter are varied from 200 nm up to 800 nm. More than 90% of the domain diameter is comparable to or even over the film thickness. Only a very small number of domain diameter exceeds 1 µm. A possible reason may be that during phase demixing, the PFO domains located in regions with a lower crystalline fraction of P(VDF-TrFE) coarsen faster and therefore, the domain size becomes extremely large.

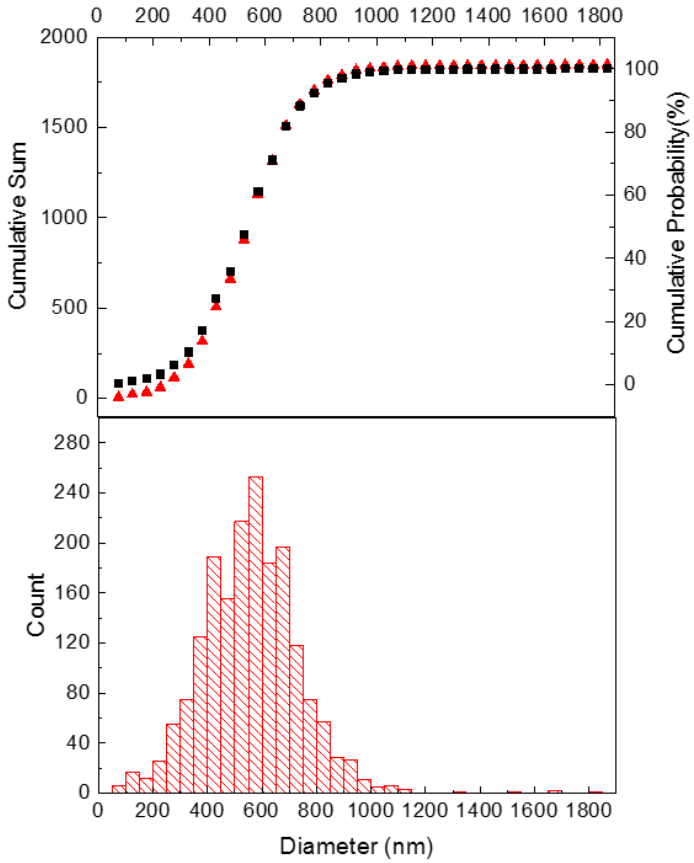

Figure 21. PFO domain diameter distribution. Upper: cumulative sum (read triangle dot) and cumulative probability (black square dot). Bottom: histogram.

4.1.2 Hexyl-PCDTBT/P(VDF-TrFE) blend

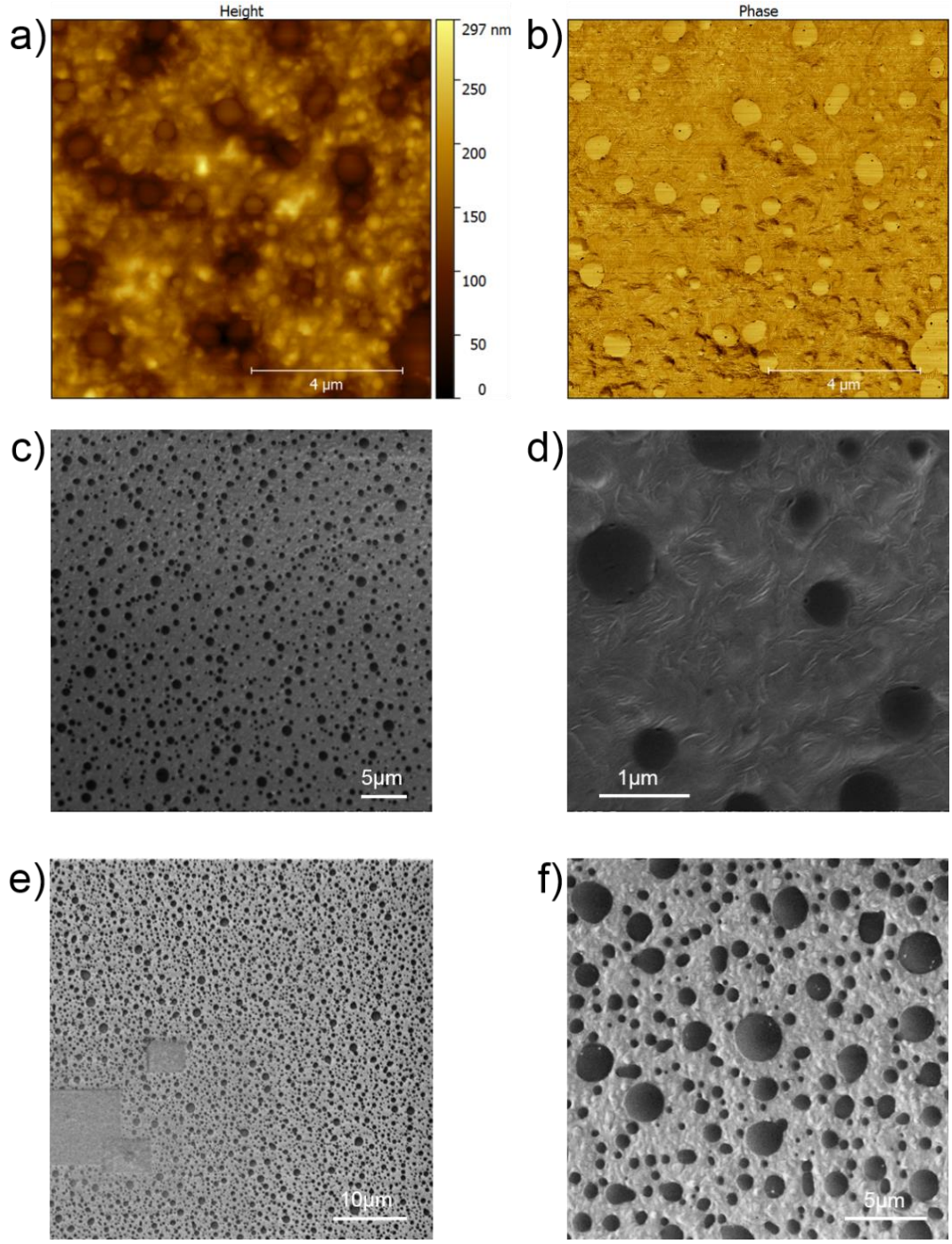

Figure 22. a) b) AFM images of a film of Hexyl-PCDTBT/P(VDF-TrFE) blends (1:9 w/w ratio, 26.6 mg/mL) on gold after annealing at 140 °C. SEM images of a film of Hexyl-PCDTBT/P(VDF-TrFE) c) d)1:9, e) f)1:4 blends on gold after annealing at 140 °C.

The surface morphology of Hexyl-PCDTBT/P(VDF-TrFE) blends film was investigated by AFM and SEM. Figure 22a,b show the resulting AFM topological image and Figure 22c-f show the top view SEM of the Hexyl-PCDTBT/P(VDF-TrFE) blends of 26~28 mg/mL with different semiconductor/ferroelectric polymer weight ratio after annealing. The film thickness amounted to 240~270 nm. The Hexyl-PCDTBT/P(VDF-TrFE) blends form a phase-separated morphology very similar to

PFO/P(VDF-TrFE). Circular-shaped Hexyl-PCDTBT (bright particles in AFM phase image) domains are randomly distributed in the P(VDF-TrFE) matrix. On a film of 1:9 weight ratio the large domains with average diameter 700 nm located below those small domains with average diameter 400 nm showing in the AFM height image. The hills and valley topology gives rise to a large surface roughness that is comparable to the layer thickness. SEM images exhibit an obvious contrast difference between domains and matrix. Black dots semiconductor Hexyl-PCDTBT are discrete and surrounded by the grey ferroelectrics matrix. The typical morphology of P(VDF-TrFE) crystal is needle-shaped structure shown in Figure 22d. The boundary between Hexyl-PCDTBT domains and P(VDF-TrFE) is easy to identify. During solvent evaporation, due to the incompatibility between two polymers, the phase demixed nearly completely leading to an obvious phase separation of Hexyl-PCDTBT and P(VDF-TrFE). The domains become larger with the increasing Hexyl-PCDTBT content. The size difference between large domains and small domains is even obvious as the semiconductor content increases. Moreover, the “stringy” features are also shown in the SEM images, similar to the morphological observation of semiconductor/P(VDF-TrFE) system in the literature[31]. This domains arrangement occurs at short processing time, originating from an ephemeral co-continuous morphology state. These morphological observations suggest the phase separation mechanism of this semiconductor/ferroelectric polymer blends system to be spinodal decomposition instead of nucleation.

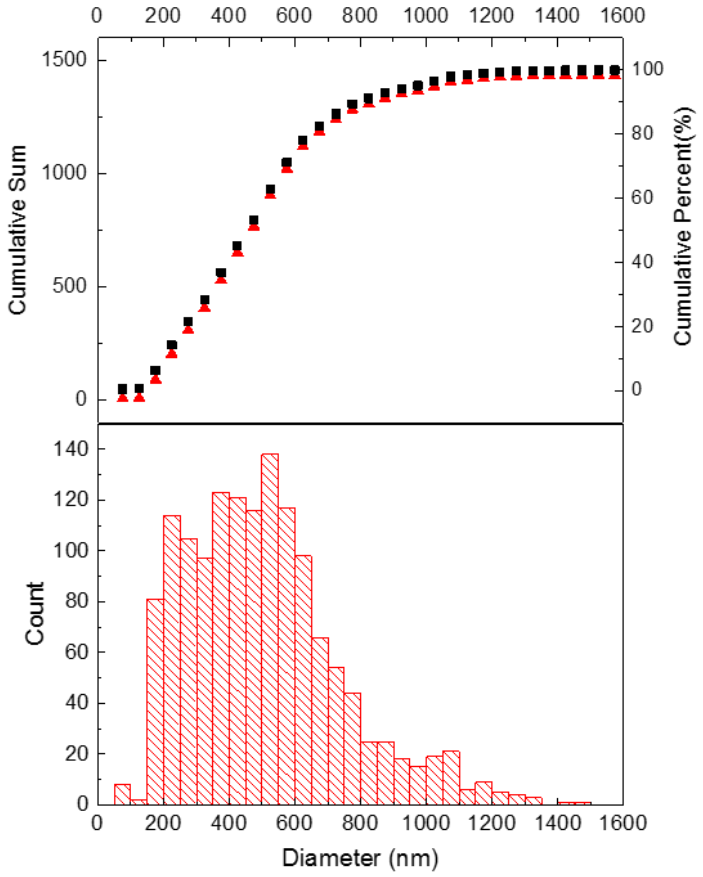

Figure 23. Hexyl-PCDTBT domain diameter distribution in 1:9 blends film. Upper: cumulative sum (read triangle dot) and cumulative probability (black square dot). Bottom: histogram.

Figure 23 shows the resulting Hexyl-PCDTBT domain diameter distribution functions form statistical analysis. A right-skewed histogram is obtained. The biggest amount of domains appears in the diameter range from 550 nm to 600 nm. Comparing with the PFO/P(VDF-TrFE) blends layer(see Figure 21), the number of domains with diameter from 200 nm to 450 nm is considerably increased. The broad size distribution is a consequence of domain coarsening during phase separation. There are more small size domains in Hexyl-PCDTBT/P(VDF-TrFE) blends film and more than 80% of domains have a lateral dimension larger than film thickness.

4.1.3 SF-PCDTBT/P(VDF-TrFE) blend

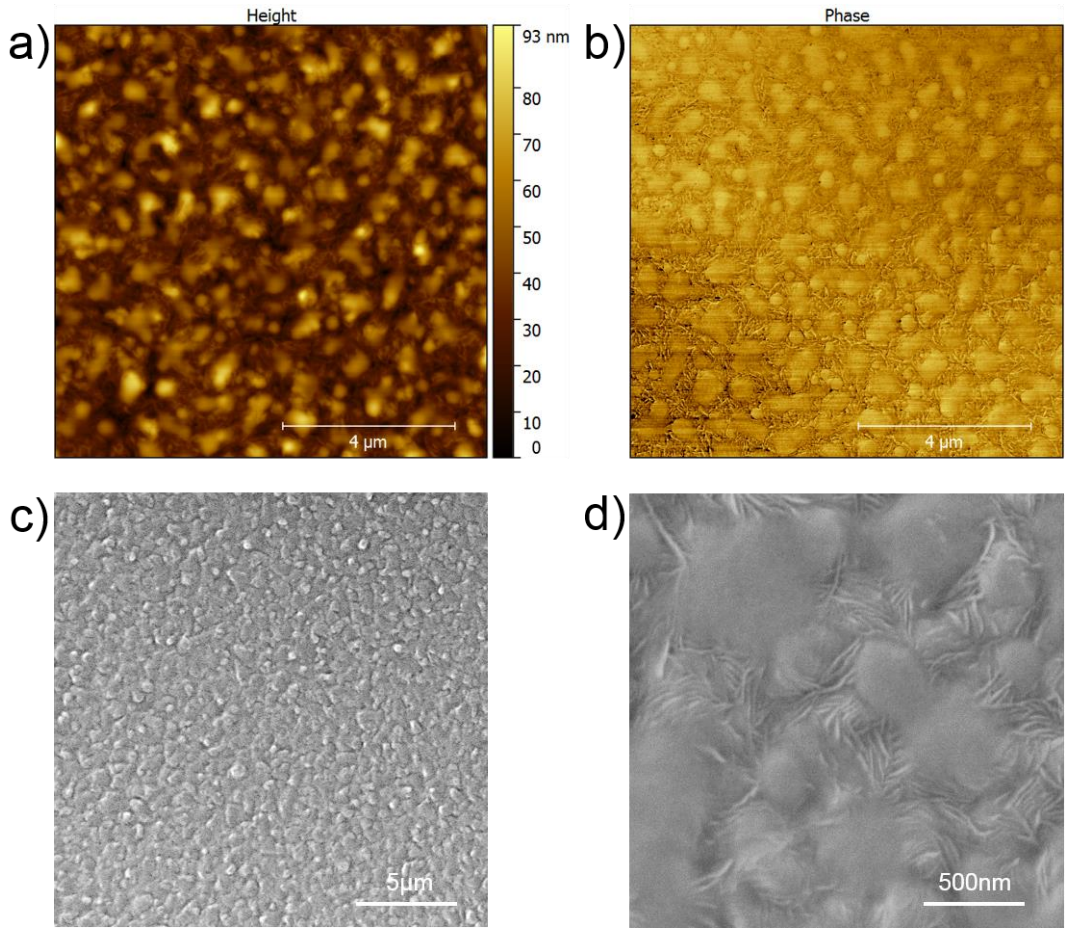

Figure 24. a) b) AFM images of a film of SF-PCDTBT/P(VDF-TrFE) blends (1:9 w/w ratio, 27.1 mg/mL) on gold after annealing at 140 °C. c) d) SEM images of a film of SF-PCDTBT/P(VDF-TrFE) blends (1:9 w/w ratio, 27.2 mg/mL) on gold after annealing at 140 °C.

Figure 24 shows the morphology of annealed SF-PCDTBT/P(VDF-TrFE)(1/9 wt/wt) polymer blends films probed by AFM and SEM. With a concentration of 26~28 mg/mL, the film thickness is about 250~290 nm. The morphology deviates strongly from the “classical” phase-separated morphology of semiconductor/ferroelectrics system. Unlike the polymer blends films mentioned above, here the domain shape is not generally circular: some domains are rather fuzzy and broad, others are circular shape with blurry boundary. Around domains

are typical needle-like semi-crystalline P(VDF-TrFE). The AFM height image reveals a reduced roughness compared with Hexyl-PCDTBT- and PFO based blends layer. It seems that all the domains protrude from the ferroelectric matrix, although we cannot exclude the presence of an amorphous top-layer of P(VDF-TrFE). SEM images elucidate that same morphology could be seen even in large scale. The detailed microstructure of the demixed blends is given in Figure 24d. The SF-PCDTBT is more intermixed with the crystalline P(VDF-TrFE). As solvent evaporating, blends phase separates with two compositions, reaching thermal equilibrium states. One is semiconductor-rich phase containing a small number of ferroelectrics and another is the ferroelectrics-rich phase with a small amount of semiconductor. Semi-fluorinated side chains might attribute to the uncommon morphology. The repulsive molecular interaction between SF-PCDTBT/P(VDF-TrFE) has been weakened by the modified semi-fluorinated octyl side chains, in comparison to the hexyl and octyl side chains of Hexyl-PCDTBT and PFO. As a consequence, polymer blends exhibit better miscibility with part integrated microstructure.

Figure 25a-h show the SEM morphology results of annealed SF-PCDTBT/P(VDF-TrFE) blends film on Au deposited glass substrates with different weight ratio, i.e., 1:18, 1:9, 1:12 and 1:5 blends ratio respectively. Under all circumstances, the broad domains with blurry boundary were obtained. The featureless domains part mixed with needle-like shaped P(VDF-TrFE). As the content of semiconductor decreased, the size of the amorphous area becomes smaller. The distance between two irregular-shaped areas extended. The 12:1 blends film exhibits similar morphology to the 9:1 blends film. Unlike the 18:1 blends film, on which the amorphous parts are discrete, the amorphous domains on the blends film with higher semiconductor content are connected somehow. In the images of the 5:1 polymer blends film, two types of amorphous domains are observed. One is with darker color and random shape, the other is with circular shape. The random shape domains are surrounded by small circular domains. However, the boundary between crystalline ferroelectrics and semiconductor is still difficult to be defined.

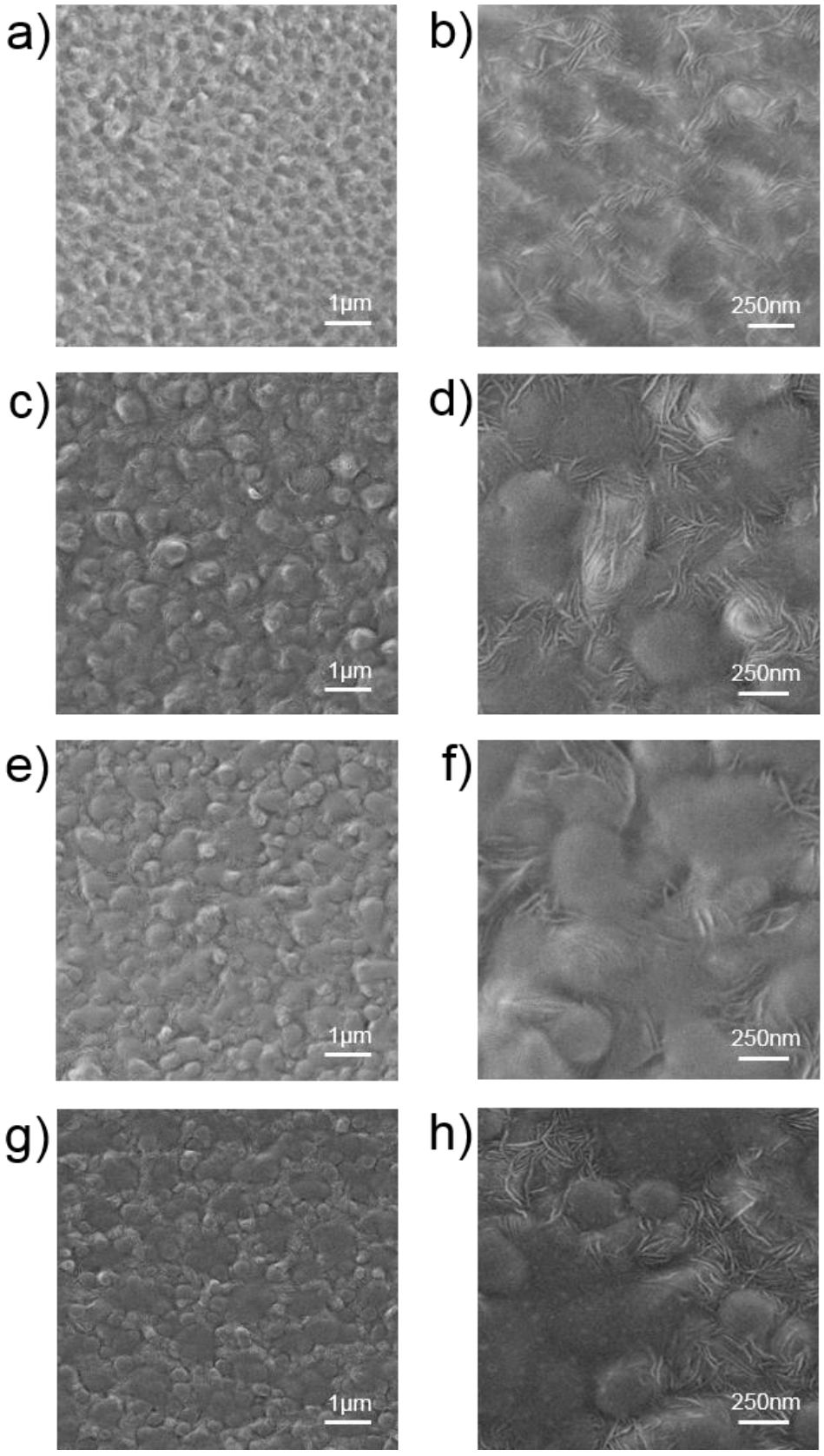

Figure 25. SEM images of the annealed films of SF-PCDTBT/P(VDF-TrFE) blends a) b) with 1:18 w/w ratio, c) d) with 1:12 w/w ratio, e) f) with 1:9 w/w ratio, g) h) with 1:5 w/w ratio on gold.

4.2 Selective dissolution

The 9:1(wt/wt) blends film of semiconductor PFO, SF-PCDTBT and Hexyl-PCDTBT, and the ferroelectrics P(VDF-TrFE) were studied for selective dissolution. The film was spin-cast from 26~28 mg/mL THF on gold-deposited glass substrate and annealed at 140 °C for two hours. All technique was explained in the experimental section. Selective dissolution treatment aims to investigate the 3D structure of polymer blends film at the micrometer scale. Specific solvent, in this case, DMSO and toluene were used to selective dissolve the ferroelectric matrix and semiconductor components respectively. The remaining microstructures were studied by AFM and SEM. As has been studied in Khikhlovskyi's work[33], four typical types of domain are expected in blends film (see figure 12).

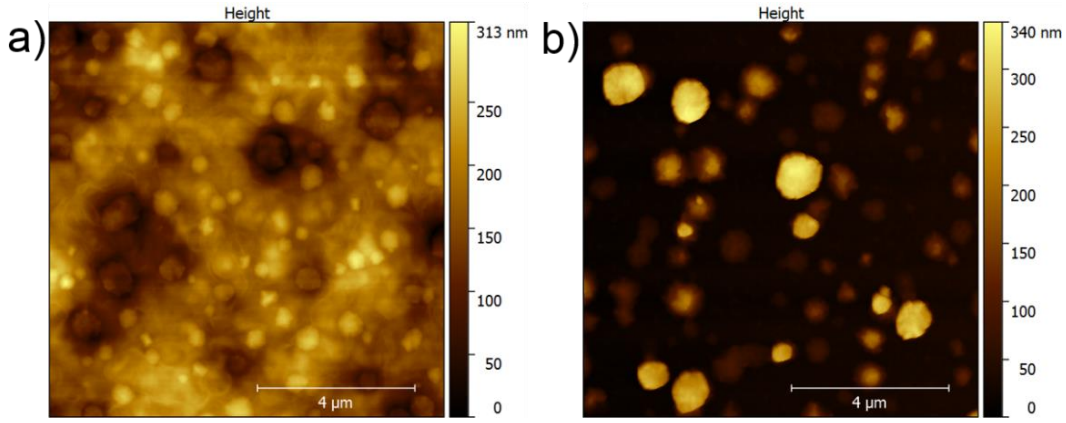

Figure 26. AFM height images of the PFO/P(VDF-TrFE) blends (1:9 w/w ratio, 26.7 mg/mL) on gold. a) the pristine control. b) the remaining topology of the blends after DMSO treatment.

In the AFM height images in Figure 26, the domains that penetrate through the film (mentioned as type 1 below), the domains that buried by matrix (mentioned as type 3 below) and the domains that float on top of the film (mentioned as type 4 below) are identified. The type 1 domains are dark color circular part in Figure 26a. They are electrically functional domains after depositing top electrode and located below the height of the matrix component. The type 3 domains are brighter but smaller circular shape which does not have any contact with the glass substrate and just protrude from matrix. Figure 26b shows the AFM height scan after DMSO treatment. The ferroelectric matrix was removed by solvent, resulting in the removal of type 2 and type 4 domains. The type 1 domains are the brightest part and produce a large altitudinal difference. We note that the type 3 domains become visible in this case indicating an altitude varied from 100 nm to 250 nm.

The results from SEM supported the existence of type 1 and type 4 further. Toluene dissolved PFO selectively and the matrix remained. In Figure 27, large contrast difference distinguished the position that semiconductor situated and the ferroelectrics matrix. All black circular area display a white border around its interface with the matrix which improved that the domains have been washed away. If we zoom into a small scale, the circular shape with the different shade of color

could be observed. Only the darker color ones are truly bridging from top to bottom substrate and occupied by the type 1 semiconductor domains. Ones with shallower color and smaller in size do not contact with the substrate that occupied by the type 3 domains. However, in this selective dissolution experiment, it is unable to detect the occurrence of type 2 domains which would not identify in pristine polymer blends film. The type 2 domains either buried in the polymer blends film or removed with matrix together upon selective washing.

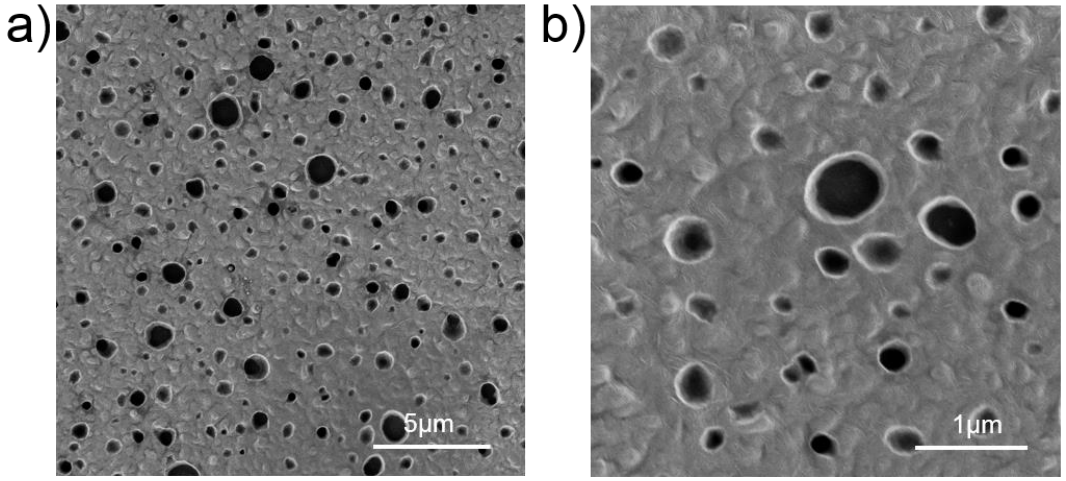

Figure 27. SEM height images of the PFO/P(VDF-TrFE) blends (1:9 w/w ratio, 27 mg/mL) on gold. a) b) the remaining microstructure of the blends after toluene treatment.

Figure 28 shows the selective dissolution results of Hexyl-PCDTBT/P(VDF-TrFE) blends film. Figure 28a is the AFM height image after DMSO treatment. Only the type 1 and the type 4 domains could be observed. Compared with PFO/P(VDF-TrFE) blends film, the number of the type 4 domains is significantly increased, which means more semiconductor in the case are buried underneath the film. This might consequently affect the device performance. The buried domains are featureless while the domains with higher altitude are circular that further prove the existence of the bridging type 1 domains.

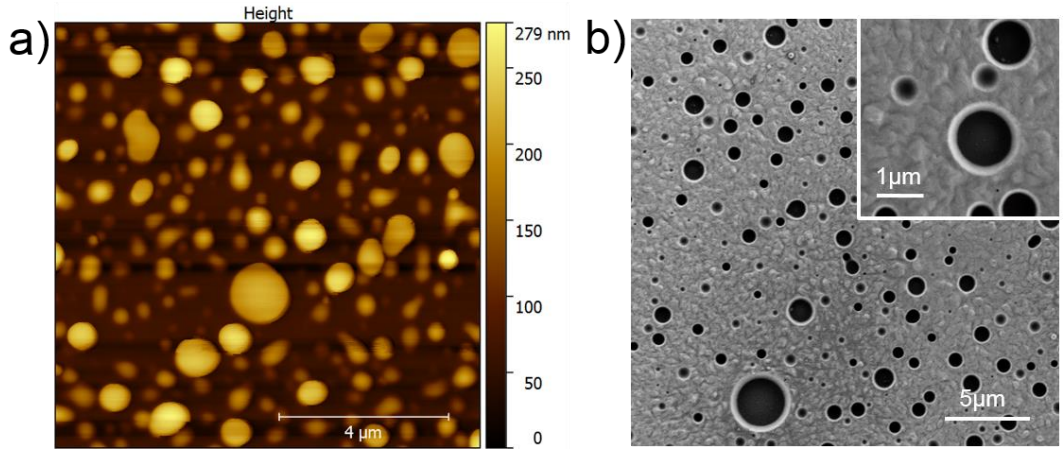

Figure 28. The remaining microstructure of the Hexyl-PCDTBT/P(VDF-TrFE) blends (1:9 w/w ratio) on gold: a) AFM height image after DMSO treatment. b) SEM images after toluene treatment.

Figure 28b presents the SEM images after Toluene treatment has been carried out on blends film. The inset image shows detailed morphology on a smaller scale. During dissolution, the reddish samples faded quickly away which could be explained by SEM results. Hexyl-PCDTBT polymer has good solubility in toluene and the type 1, as well as the type 3 domains, were removed from substrates. There is a correlation between the size of drop-like domains with a white border and its contrast. The domains with a larger diameter are darker than the domains with a smaller diameter. The observations in Hexyl-PCDTBT/P(VDF-TrFE) blends films agree with the PFO/P(VDF-TrFE) case. The darker domains are type 1 penetrate through the whole film whereas the shallower domains just are the “floating” type 3 protruding out the surface. As the solvent evaporates, the demixing polymer blends did phase separate which is subsequently arrested by vitrification of organic semiconductor[38], developing into discrete Hexyl-PCDTBT domains and P(VDF-TrFE) matrix.

The selective dissolution results of SF-PCDTBT/P(VDF-TrFE) blends film are shown in Figure 29. Figure 29a,b are the AFM scan after DMSO treatment. The ferroelectric matrix was removed by the solvent. Unlike previous polymer blends film, there are large numbers of remaining domains. Some domains formed a circular shape and have higher altitude. The other is arbitrary and seem to be the type 3 domains underneath the matrix. The average domain size is evidently smaller then PFO and Hexyl-PCDTBT domain size. Considering the film thickness, the type 1 domains are barely seen within the field of view.

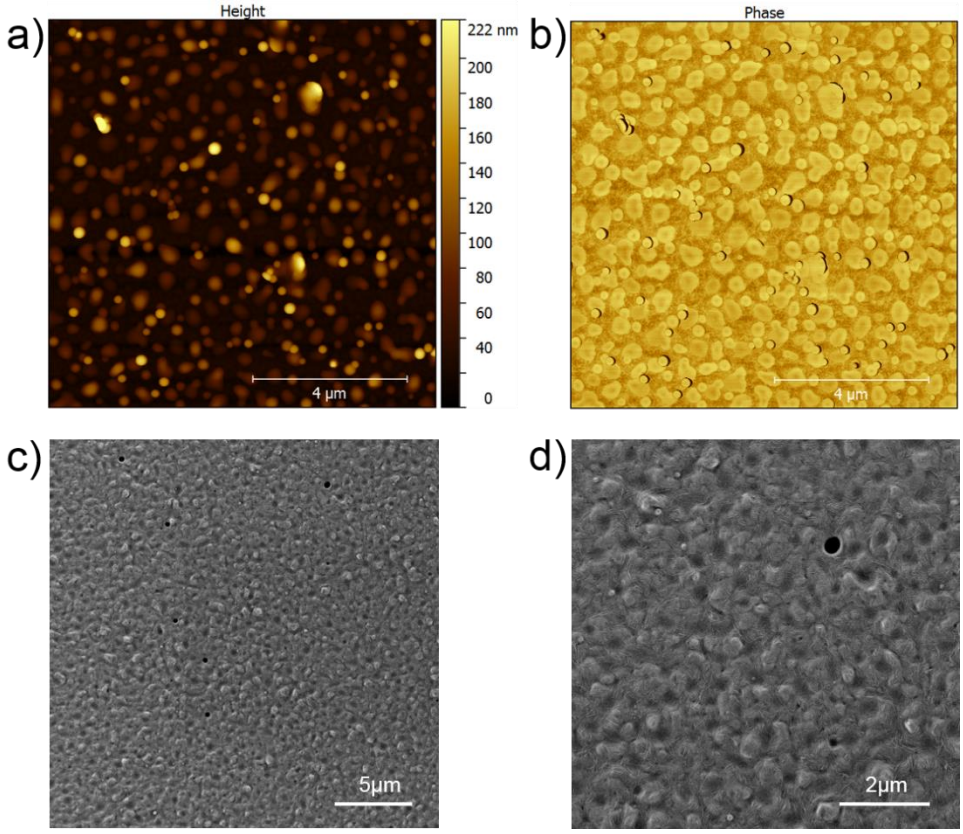

Figure 29. The remaining microstructure of the SF-PCDTBT/P(VDF-TrFE) blends (1:9 w/w ratio) on gold: a) b) AFM height and phase image after DMSO treatment. c) d) SEM images after Toluene treatment.

4.3 Electrical Characterization

The electrical characterization was carried out under an ambient condition of 23 °C. Au and Al were chosen as the electrode. The work function of Au electrode is 4.7 eV and Al electrode is 4.1 eV. The energy levels of the used semiconductors are listed in Table 2 Due to the semi-fluorinated side chains the HOMO level of SF-PCDTBT is 0.3 eV lower than hexyl-PCDTBT as they result in an additional out-pointed surface dipole moment[39]. The injection barrier from Au into PFO, hexyl-PCDTBT and SF-PCDTBT is in the order of 1.3 eV, 0.6 eV and 0.9 eV. The memory bits dimension amounted to 0.4 mm×0.4 mm (see Figure 16b the intersection of the yellow line and the grey line).

Table 2. Energy levels of semiconductor used in experiment.

Polymer	HOMO	LUMO
PFO	-6.0eV	-2.9eV
Hexyl-PCDTBT	-5.3eV	-3.3eV
SF-PCDTBT	-5.6eV	-3.6eV

4.3.1 PFO based memory diode

We noted that film thickness plays an important role since the device with 180± 5 nm blend film all got short without the protection of PEDOT:PSS. Here, we only show the current-voltage measurement result of 180 nm PFO/P(VDF-TrFE) blends film device with PEDOT:PSS layer on top.

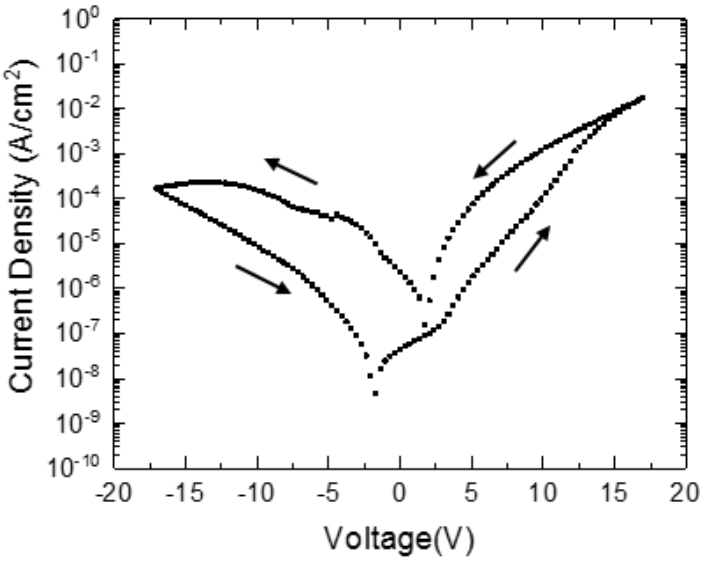

Figure 30. I-V sweep of the PFO/P(VDF-TrFE) 1:9 blends device with PEDOT:PSS protected layer.

Bias was applied on the Au electrode while the top electrode Al was grounded. The current density was plotted by an exponential y-axis. Figure 30 shows a typical I-V sweep with the testing voltage range from - 17 V to + 17 V beyond which an unstable curve or even device short was obtained. As increasing the voltage from 0 V in the positive bias, the current increased in the meantime. At about 12-15 V, the current rose suddenly. Upon sweeping back from high voltage to low voltage, the current remained high until there is no applied bias. In the negative bias, when the voltage swept from 0 V to - 17 V, the current still increased to a high value. However, a slower rise was observed after - 10 V. Then, the current was at a lower value when the voltage swept back. The current-voltage curve showed a typical hysteresis loop of phase-separated ferroelectric-semiconductor polymer blend memory device and the loop seems symmetric.

Increasing the polymer blends solution concentration is consequently thickening layer thickness. With higher concentration, we got 220-nm-thick blends film. Thus, PEDOT:PSS protecting layer is not necessary for the devices.

Figure 31 demonstrates I-V sweep process during the measurement. The switching property of devices was observed. Under low voltage pulses of ± 5 V (see Figure 31a), hysteresis loop was clockwise in the positive bias and counterclockwise in the negative bias. The current density values were low, ranging from 10^{-11} to 10^{-8}. At a bias of ± 7 V (see Figure 31b), loop changed direction to counterclockwise in the positive bias and current reached a higher value. In the reverse bias, the current value remained low. As the voltage increases, the loop area becomes larger since the current difference between the curve sweeping from 0 V to larger voltage and the curve that swept back is increased in the positive bias. It indicates that the ferroelectrics in this device is poled improving charge injection gradually. However, there is not an obvious change in the current value in this process.

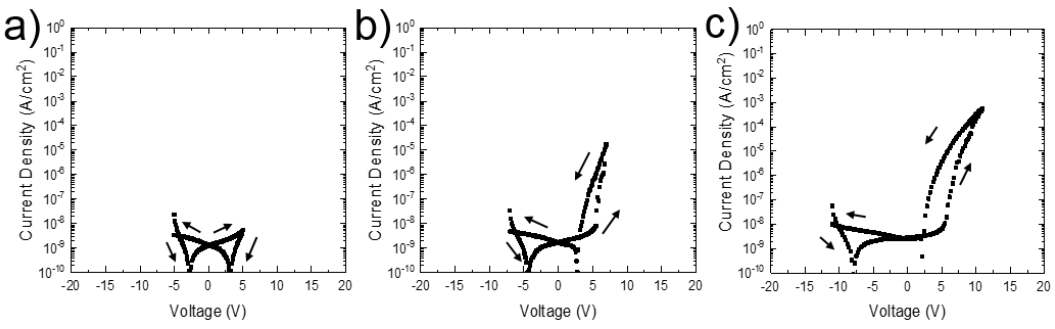

Figure 31. Switching behavior in forward bias of the device based on the PFO/P(VDF-TrFE) 1:9 blend; panels a),b) and c) represent the IV data scanned up to a voltage of 5,7 and 12 V, respectively.

The largest bias that could be applied on this PFO/P(VDF-TrFE) blends device was ± 22 V since the devices burnt at even higher voltages. The I-V sweep result is presented in Figure 32a. In forward bias, the current is bistable with increased voltage. The coercive voltage appeared at around 12 V and a relevant current growth is shown. The device is switched from low conductive OFF-state into high conductive ON-state. In the reverse bias, the low current is governed by leakage

that shows the switching from ON-state to OFF-state. The Au electrode is injecting contact for charges while aluminum is blocking contact that function together with PFO/P(VDF-TrFE) blends film forming a switchable diode.

To reveal electrical transport at switched mode, voltage pulses of ± 21 V, i.e. is larger than the coercive voltage was applied on the device. The current-voltage measurement was carried out between - 5 V and + 5 V, as presented in Figure 32b. When the device was pulsed at + 21 V, the ferroelectrics were poled reversely against applied bias and Au contact improved charge injection. The device was switched to low-resistive ON-state. When the device was pulsed at – 21 V, the device was poled into high resistive OFF-state. The resulting ON/OFF ratio was about three orders of magnitude. The asymmetry curve is due to Al blocking contact. The obtained ON/OFF ratio for this memory device goes 2923 which is about ten times smaller than the values in previous study[30].

The switching function relies on the phase separation of PFO/P(VDF-TrFE) blends that PFO forms a continuous phase contacting with both electrodes as demonstrated by AFM and SEM images. The current flows through an nm-scale distance at the semiconductor/ferroelectrics interface.

For memory device, the data retention is a crucial property indicating the stability of one device. The data retention is dominantly related with the ferroelectric depolarization. As long as the applied field larger than the coercive field, the polarization is stable and the charge compensation at blends interface takes place continuously. Upon decreasing the field strength, the ferroelectric starts to depolarize, the current declines gradually until the diode becomes the initial unpoled state. Since the read-out voltage is much lower than the coercive voltage, the data retention leaks away as time proceeds. During the measurement, the device was first polarized in ON-state by a high pulse and measured as set intervals. The OFF-current measurement followed the same procedure. The data retention time dependence is shown in Figure 32c. The ON-current degraded from 8.4^{-8} A to 3.1^{-9} A whereas the OFF-current seems more stable.

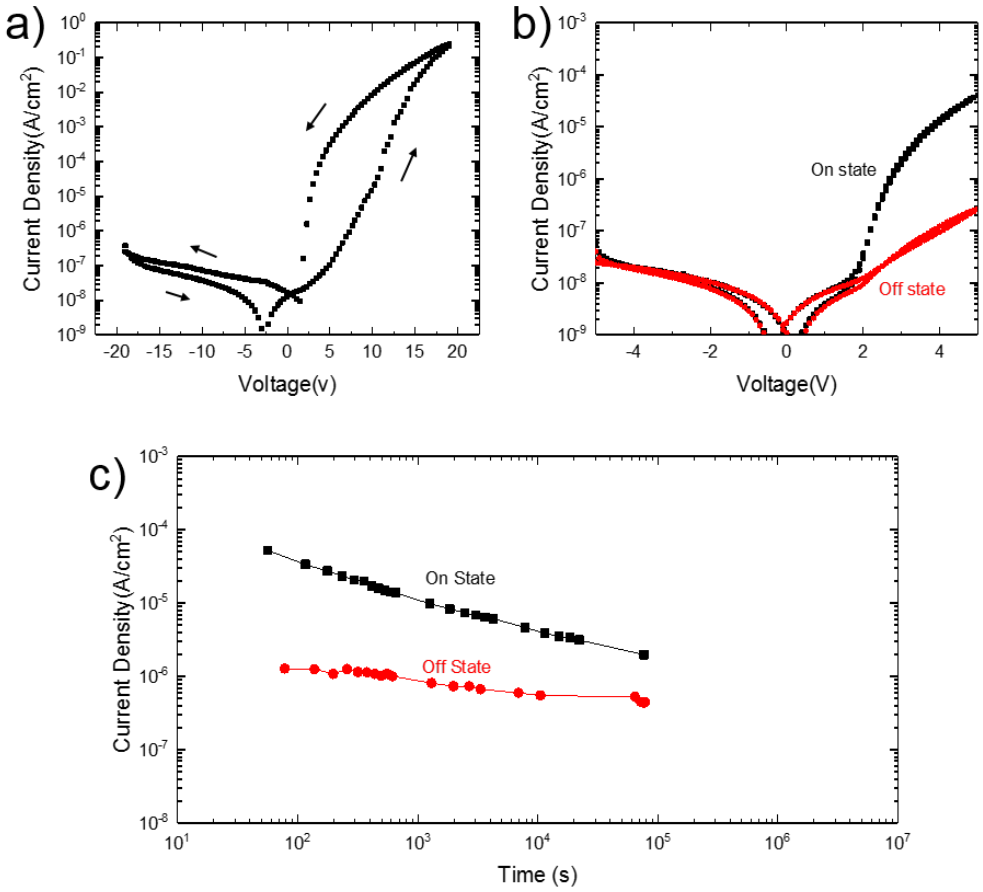

Figure 32. Electrical characterization of PFO/P(VDF-TrFE) 1:9 blends device: a) I-V sweep shows the typical hysteresis loop in forward bias. b) low voltage read-out. c) data retention after programming the device in either ON-state or OFF-state.

4.3.2 Hexyl-PCDTBT based memory diode

The I-V sweep process for the Hexyl-PCDTBT/P(VDF-TrFE) device was shown in Figure 33. External voltage was applied on the Au electrode. Interestingly, a clockwise hysteresis loop appeared at low voltage in both positive- and negative bias, which means that switching of ferroelectric polymer occurred, resulting in charge injection from Al electrode at the ferroelectric/semiconductor interface. The injection barrier from Al into the HOMO of Hexyl-PDCTBT is about 1.2 eV that can be surmounted by ferroelectric rectification according to previous research[40]. Up to 7 V, the switching behavior was exhibited in the positive bias with small area hysteresis loop.

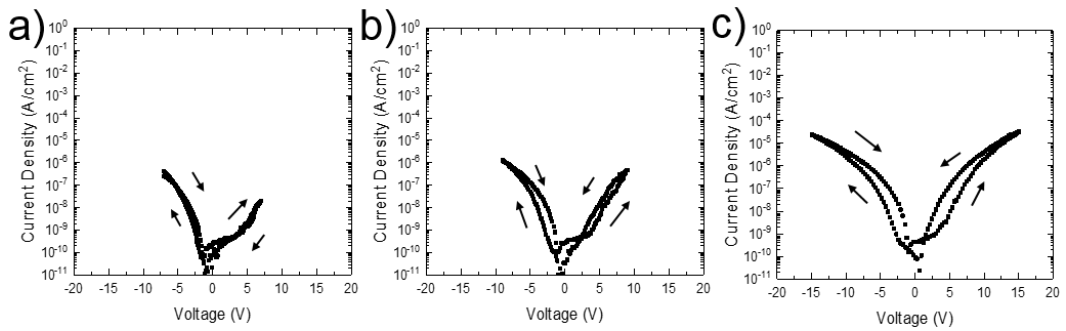

Figure 33. Switching behavior in forward bias of the device based on the Hexyl-PCDTBT/P(VDF-TrFE) 1:9 blend; panels a),b) and c) represent the IV data scanned up to a voltage of 7,10 and 15 V, respectively.

In forward bias, the voltage is swept from 0 V to 18 V (shown in Figure 34a). As the voltage increased, the current increased simultaneously. Owing to the charge injection limitation from the Au electrode, the current is low and the device is in the high resistive OFF-state. Upon increasing the bias beyond coercive voltage, in this case about 12 V, the ferroelectric polymer P(VDF-TrFE) are all polarized into the same direction that is reverse the applied field. The charge injection is encouraged and therefore the device is in the ON-state. When sweeping back to 0 V, the high current density is maintained since the ferroelectric remains polarized. At negative bias, a comparable curve was observed even the device layout is asymmetric. We noticed that the hysteresis loop covered less area than the hysteresis loop of PFO/P(VDF-TrFE) device, leading to a small ON/OFF ratio about 23 . During measuring, the device performance was not stable, the device easily short-circuited after several current-voltage sweeps.

Figure 34b plot the retention over a day. The ON-current dropped gradually from 2.1^{-10} A to 1.8^{-11} A. After 10^4 s, it shows fluctuation and finally decreased to 9.8^{-12} A. The OFF-current was stable at the first stage. After 10^4 seconds the OFF-current rose to 5.9^{-12} A exceeding the ON-current. The growth trend remains even at the end of the measurement.

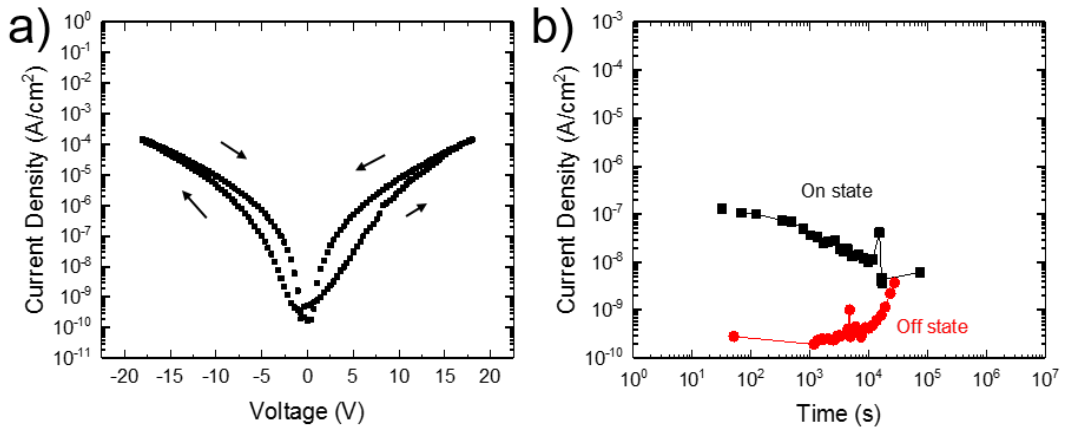

Figure 34. Electrical characterization of Hexyl-PCDTBT/P(VDF-TrFE) 1:9 blends device: a) I-V sweep shows the typical hysteresis loop in both biases. b) data retention after programming the device in either ON-state or OFF-state.

4.3.3 SF-PCDTBT based memory diode

Figure 35 indicates the switching process behavior at both biases. As the voltage increased at the forward bias, the P(VDF-TrFE) was gradually polarized. At about 15 V, the hysteresis loop first changed from clockwise to counterclockwise direction. Switching also took place at negative bias although the appearing voltage is smaller than the switching at positive bias. This can be addressed by the smaller injection barrier from Au into HOMO of SF-PCDTBT. At about 25 V, two hysteresis loop at both biases could be observed.

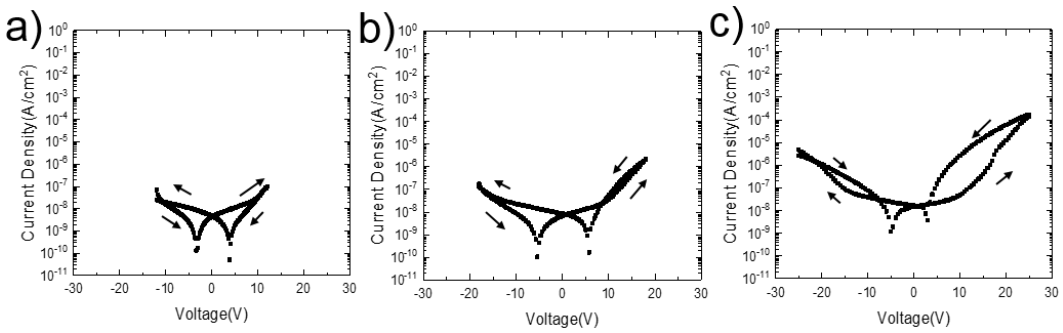

Figure 35. Switching behavior in both biases of the device based on the SF-PCDTBT/P(VDF-TrFE) 1:9 blend; panels a), b) and c) represent the IV date scanned up to a voltage of 10,20 and 25 V, respectively.

Figure 36a is the current-voltage measurement sweeping from -35 V to +35 V. At about 18 V, the device switched from the OFF-state to the ON-state. The ON/OFF ratio under forward bias is 1900 which is comparable with PFO/P(VDF-TrFE) device. However, in reverse bias, the ON/OFF ratio, which is 106, is one order of magnitude lower than in forward bias. Like PFO/P(VDF-TrFE) device, the SF-PCDTBT/P(VDF-TrFE) device can be programmed to show bistability by applying pulse and the results are given in Figure 36b. Depending on the polarity, the device is either at high resistance ON-state or low resistance OFF-state. The non-volatile readout can be realized at low voltage. Figure 36c shows the retention time of ON- and OFF-state. The ON-state current decreased from 1.8^{-8} A to 3.8^{-10} A. The OFF-current was stable at 2^{-11} A for more than 7×10^{4} s and no growth was observed.

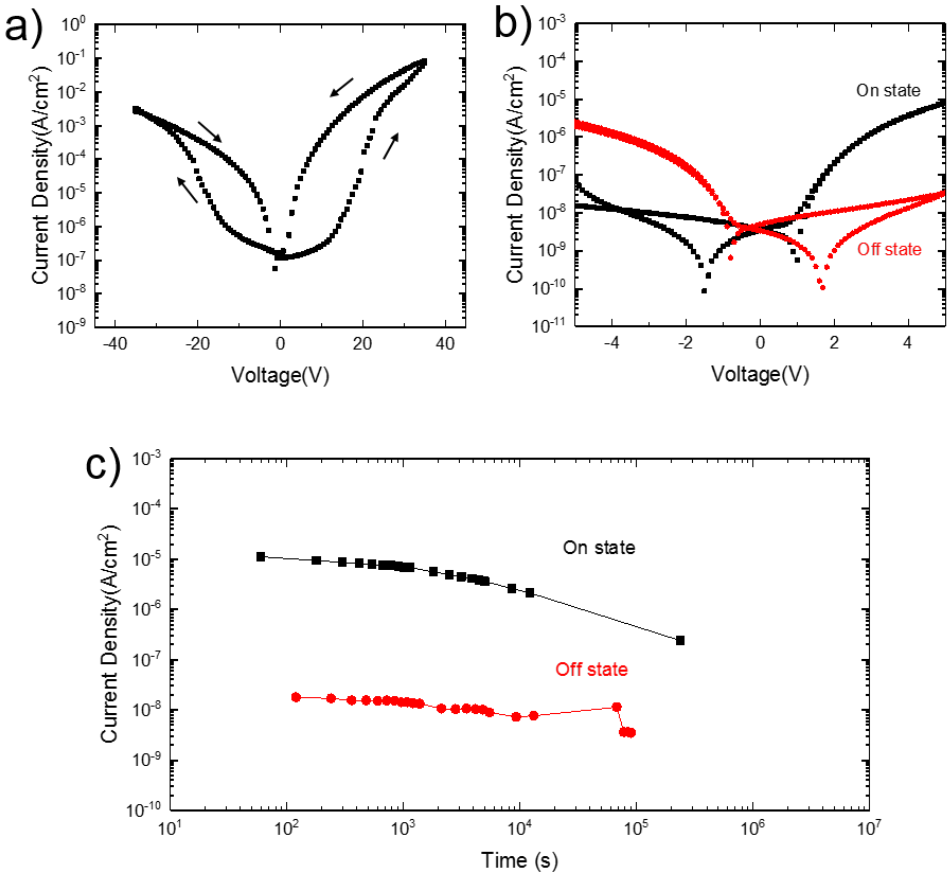

Figure 36. Electrical characterization of SF-PCDTBT/P(VDF-TrFE) 1:9 blends device: a) I-V sweep shows the typical hysteresis loop in both biases. b) low voltage read-out. c) data retention after programming the device in either ON-state or OFF-state.

A series of devices was fabricated by varying SF-PCDTBT content in the polymer blends. The I-V sweep with each SF-PCDTBT content is demonstrated in Figure 37. For all memory devices, the current-voltage curve shows the butterfly-shaped hysteresis loop in positive- and negative bias, in accordance with the result of 1:9 ratio blends device. The devices are working even with low SF-PCDTBT content. Upon increasing the voltage beyond the coercive voltage, the devices are switched from low conductive state into high conductive state. The sweeping bias depends on the thickness of the blends film, i.e. 190 nm for 1:5 w/w ratio film, 300 nm for 1:12 w/w ratio film and 230 nm for 1:18 w/w ratio film. The ON/OFF current ratio in forward bias of memory diodes as a function of different weight ratio of SF-PCDTBT/P(VDF-TrFE) polymer blends film is presented in Figure 37d. We note that as the content of SF-PCDTBT polymer increases, the ON/OFF ratio shows a noticeable upward trend up to 10 wt% but falls slightly for larger SF-PCDTBT content. Despite the fact that the phase separation morphology for the SF-PCDTBT/P(VDF-TrFE) is very different from the “classical” morphology, the best performing ratio remains 1:9 and is almost one hundred times larger than the ON/OFF current in the ratio of 1:18. The film surface profile was measured by DEKTAK profilometer with a length of 2 mm (see Figure 38). The ten-point mean roughness reveals a value of 43.3 nm of 1:5 film, 20.2 nm of 1:9 film and 18.3 nm of 1:12 film, respectively. The roughness grows with the increasing SF-PCDTBT content, resulting in a coarse film. In addition, in the ON-state, the stray field in the ferroelectrics is in the opposite direction to the external electric field. Hence, the

effective field with higher P(VDF-TrFE) is undermined and the corresponding current is lower[29].

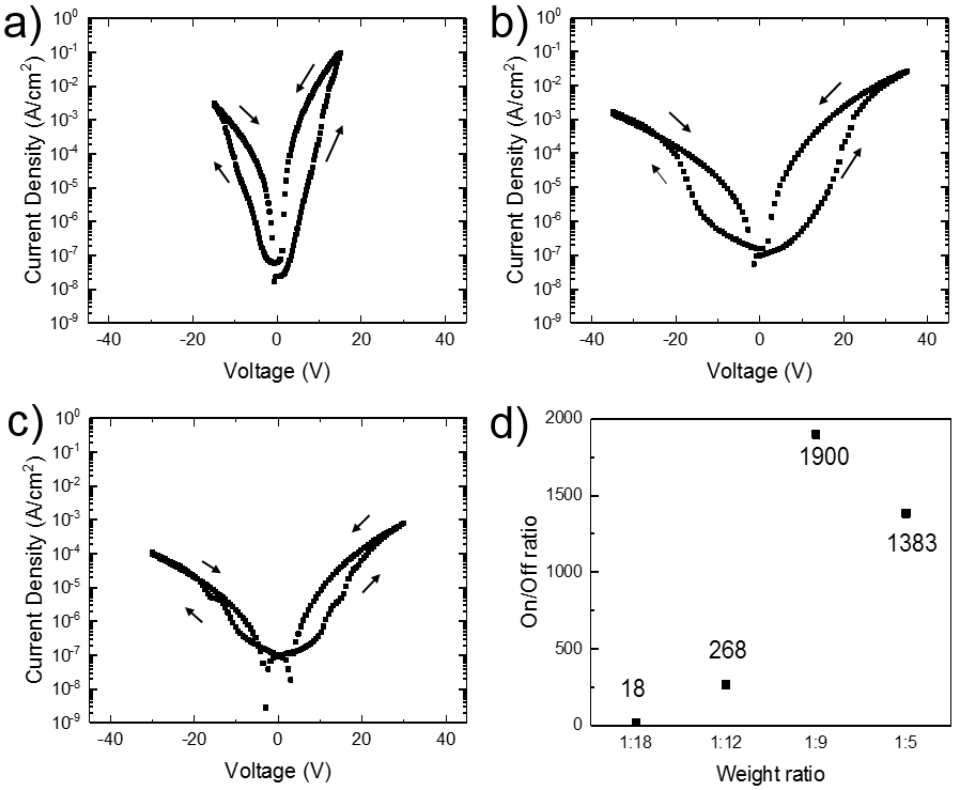

Figure 37. I-V sweep of SF-PCDTBT/P(VDF-TrFE) blends devices: a) with 1:5 weight ratio; b) with 1:12 weight ratio; c) with 1:18 weight ratio. d) ON/OFF current ratio of SF-PCDTBT/P(VDF-TrFE) blends devices versus 1:18, 1:12, 1:9, 1:5 semiconductor: ferroelectric weight ratio.

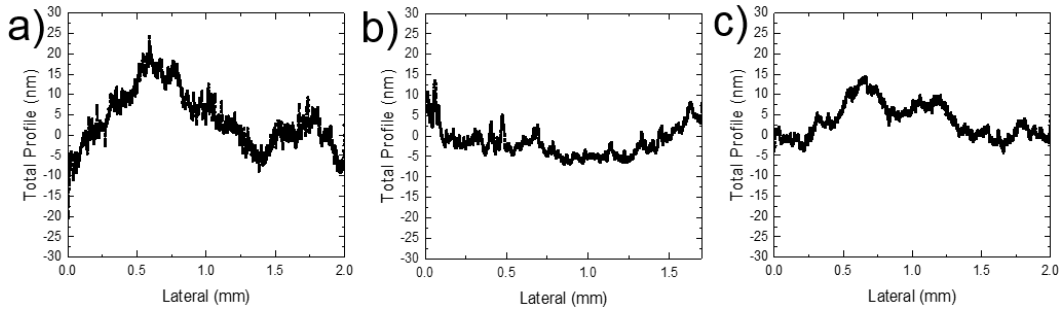

Figure 38. The surface roughness of SF-PCDTBT/P(VDF-TrFE) blend layer: a) with 1:5 weight ratio. b) with 1:9 weight ratio. c) with 1:12 weight ratio.

The device performance of three types of memory diode is concluded in Table 3. For each type of ferroelectric diode, the blend weight ratio, film thickness and the ON/OFF ratio are presented. For the PCDTBT based memory diode, the ON/OFF ratio is recorded at positive and negative bias which is expressed as “+” and ”-”.

Table 3. Summary properties of memory diode base on PFO-PCDTBT/P(VDF-TrFE), Hexyl-PCDTBT/P(VDF-TrFE) and SF-PCDTBT/P(VDF-TrFE) blend. “+” and “-” refer to the positive and negative bias, respectively.

Semiconductor	Ferroelectrics	Weight ratio	Film thickness(nm)	ON/OFF “+”	ON/OFF “-”
PFO	P(VDF-TrFE)	1:9	220	2923	/
Hexyl-PCDTBT	P(VDF-TrFE)	1:9	240	23	/
SF-PCDTBT	P(VDF-TrFE)	1:5	190	7	1383
SF-PCDTBT	P(VDF-TrFE)	1:9	285	1900	106
SF-PCDTBT	P(VDF-TrFE)	1:12	300	268	34
SF-PCDTBT	P(VDF-TrFE)	1:18	230	18	4

4.3.4 Electroluminescence

In an organic light emitting diode, the light emission is in response to an electric current. The functional layer is sandwiched between two electrodes. When an electric field is applied, if the electrons injected into LUMO of the organic at the cathode and the holes are injected into HOMO of the organic layer at the anode. They will recombine by electrostatic force forming an exciton. As the excited state decays, the energy releases which is accompanied by light emitting. However, if the device is only holes injected or electrons injected, light emission cannot occur. In order to investigate whether both types of charge carriers are injected, electroluminescence measurements were carried out on memory diodes. The electroluminescence devices were fabricated with the same layer architecture (see Figure 17a) with blends of PFO/P(VDF-TrFE) and SF-PCDTBT/P(VDF-TrFE) 9:1. To ensure the possible detection of light emission, the thickness of Au layer is reduced to 20 nm and the device area amounted to 1 mm×1 mm (see Figure 17b). A current, which is generated after the photosensitive materials absorb the photons, is called photocurrent. The results are presented in Figure 39. This shows IV-characteristics of two PFO/P(VDF-TrFE) devices plotted by respective color(see Figure 39a). The red curve shows current vs. voltage relationship in both biases. However, the photocurrent is not reliable since the high short current was observed in this case. The electroluminescence might come from the device shortage. The black curve shows no corresponding photocurrent signal. Although there is the hysteresis loop in both bias, the ON/OFF ratio is smaller than 1, indicating that the device did not work. The work function of Al is about 4.1 eV which suppresses the electrons injection into the LUMO of PFO and thus, the device is only holes injected.

Figure 39b shows the current-voltage characterization and corresponding light emission of three SF-PCDTBT/P(VDF-TrFE) devices respectively. All current-voltage curves indicate hysteresis loop in both forward and backward bias and the area of the forward loop is larger than the backward loop. Firstly, the electrons current was trap-limited[30] leading an OFF-current that start at 11 V. The coercive voltage at which the device switches on, is about 15 V. Therefore, we observe a quite low photocurrent and no light emission. When the voltage was increased to above 15 V, hole-injection occurred and the device started to switch in ON-state. The photocurrent rose sharply and maintained upon sweeping back because the anode kept holes injecting. The holes injected from Au electrode into the HOMO of SF-PCDTBT while electrons injected from Al electrode into LUMO. The hole and electron then recombine as an exciton. When it leaves the excited state, the energy is released as the form of light. As the hole-injection process lasts, the light emission can be observed. Light emission was vanished down to +11 V. The switching voltage is unity for all devices owing to the same coercive field of the ferroelectrics.

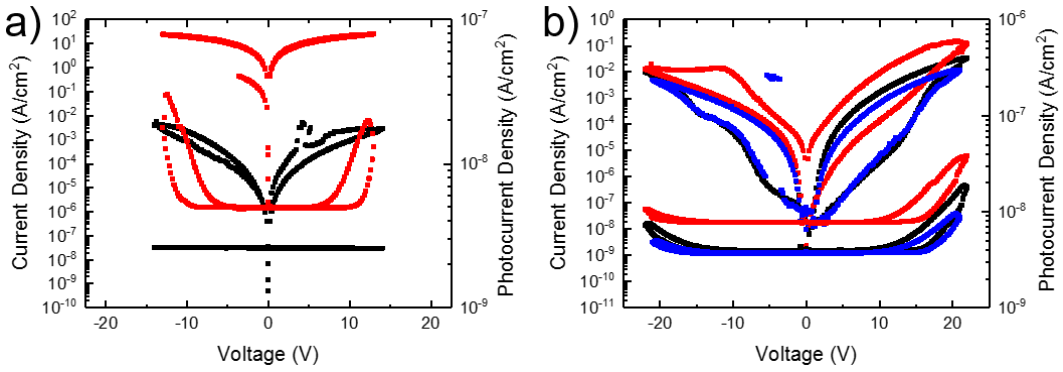

Figure 39. Opto-electrical characterization of memory diodes with a) PFO/P(VDF-TrFE) 1:9 blends devices; b) SF-PCDTBT/P(VDF-TrFE) 1:9 blends devices. The left y-axis is the current density and the right y-axis is the photocurrent density.

Conclusion

In summary, non-volatile memory devices have been fabricated, utilizing a solution-cast phase-separated blends film of semiconductor and ferroelectric polymer. Three different semiconductor polymers have been used, e.g., poly(9'9-dioctyl-fluorene), hexyl alkyl side chain modified and semifluorinated alkyl side chain modified poly[N-9'-heptadecanyl-2,7-carbazole-alt-5,5-(4',7'-di-2-thienyl-2',1',3'-benzothiadiazole)]. The morphology of spin-coated blends film was investigated by various microscopic techniques. During solvent evaporation, the morphology was formed which is neither influenced by the annealing process nor the substrate materials. The blends of PFO/P(VDF-TrFE) and Hexyl-PCDTBT/P(VDF-TrFE) phase separate completely, developing into cylindrical amorphous semiconductor domains embedded in the needle-shaped crystalline ferroelectric matrix. With the benefit of selective dissolution treatment, we indicate the typical phase separated morphology types of semiconductor domains: one is continuous from bottom to top, another is buried under the film and the other protrudes out of the film. The domains size for a given blends weight ratio is rather monodisperse and expand with the semiconductor content. These observations can be explained by the spinodal decomposition mechanism.

The SF-PCSTBT/P(VDF-TrFE) blends film, however, shows a distinctly different morphology in comparison to the "classical case" of circular domains of semiconductor embedded in the ferroelectric matrix. The morphology indeed seems to suggest that the semifluorinated side chain increases the miscibility between the semiconductor and ferroelectric polymer. Chemical characterization of the domains is ongoing and will not be part of this thesis. In contrast to both the PFO and Hexyl-PCDTBT, the spin-coated films of the SF-PCDTBT/P(VDF-TrFE) blends are quite smooth. Furthermore, the domain boundaries are fuzzy instead of sharp. The selective dissolution treatment reveals that it is difficult to wash the semiconductor away which means the SF-PCDTBT is much better mixed with the matrix.

The electrical performance of the PFO/P(VDF-TrFE) based memory device is comparable to the literature, although the ON-OFF ratio is somewhat lower. Interestingly, the Hexyl-PCDTBT/P(VDF-TrFE) blend, which has a morphology that is qualitatively comparable with that of PFO/P(VDF-TrFE) blend, only exhibited very low currents. In contrast, and perhaps surprisingly, the SF-PCDTBT/P(VDF-TrFE) blend shows very decent hysteresis loops, both in positive and negative bias. Interestingly though, the 1/9 w/w semiconductor/ferroelectric ratio still gives the best performance. In addition, electroluminescence measurements indicated that holes and electrons are injected combined in SF-PCDTBT, which upon recombination give light emission.

Reference

[1] Naber, R. C., Asadi, K., Blom, P. W., de Leeuw, D. M., & de Boer, B. (2010). Organic nonvolatile memory devices based on ferroelectricity. *Advanced materials*, *22*(9), 933-945.

[2] Asadi, K., De Leeuw, D. M., De Boer, B., & Blom, P. W. (2008). Organic non-volatile memories from ferroelectric phase-separated blends. *Nature materials*, *7*(7), 547.

[3] Valasek, J. (1921). Piezo-electric and allied phenomena in Rochelle salt. *Physical review*, *17*(4), 475.

[4] Scott, J. F. (2007). Ferroelectrics go bananas. *Journal of Physics: Condensed Matter*, *20*(2), 021001.

[5] Von Hippel, A. (1952). Piezoelectricity, ferroelectricity, and crystal structure. *Zeitschrift für Physik A Hadrons and nuclei*, *133*(1-2), 158-173.

[6] Fridkin, V., & Ducharme, S. (2014). Ferroelectricity and Ferroelectric Phase Transition. In *Ferroelectricity at the Nanoscale* (pp. 1-9). Springer, Berlin, Heidelberg.

[7] Haas, C. (1965). Phase transitions in ferroelectric and antiferroelectric crystals. *Physical Review*, *140*(3A), A863.

[8] Aizu, K. (1964). Symmetries in the paraelectric phase-transformations of ferroelectric crystals. *Journal of the Physical Society of Japan*, *19*(6), 918-923.

[9] Dawber, M., Rabe, K. M., & Scott, J. F. (2005). Physics of thin-film ferroelectric oxides. *Reviews of modern physics*, *77*(4), 1083.

[10] Scott, J. F., & De Araujo, C. A. P. (1989). Ferroelectric memories. *Science*, *246*(4936), 1400-1405.

[11] de Arquer, F. P. G., Armin, A., Meredith, P., & Sargent, E. H. (2017). Solution-processed semiconductors for next-generation photodetectors. *Nature Reviews Materials*, *2*(3), 16100.

[12] Szklarz, P., & Bator, G. (2005). Pyroelectric properties of tricyclohexylmethanol (TCHM) single crystal. *Journal of Physics and Chemistry of Solids*, *66*(1), 121-125.

[13] Eley, D. D. (1963). Organic Semiconductors. *Nature*, 197, 932.

[14] Nalwa, H. S. (1995). *Ferroelectric polymers: chemistry: physics, and applications*. CRC Press.

[15] Kepler, R. G., & Anderson, R. A. (1992). Ferroelectric polymers. *Advances in physics*, *41*(1), 1-57.

[16] Lovinger, A. J. (1983). Ferroelectric polymers. *Science*, *220*(4602), 1115-1121.

[17] Furukawa, T. (1989). Ferroelectric properties of vinylidene fluoride copolymers. *Phase Transitions: A Multinational Journal*, *18*(3-4), 143-211.

[18] Kabir, E., Khatun, M., Nasrin, L., Raihan, M. J., & Rahman, M. (2017). Pure β-phase formation in polyvinylidene fluoride (PVDF)-carbon nanotube composites. Journal of Physics D: Applied Physics, 50(16), 163002.

[19] Scheinbeim, J., Nakafuku, C., Newman, B. A., & Pae, K. D. (1979). High pressure crystallization of poly (vinylidene fluoride). *Journal of Applied Physics*, *50*(6), 4399-4405.

[20] Arkhipov, V. I., Von Seggern, H., & Emelianova, E. V. (2003). Charge injection versus space-charge-limited current in organic light-emitting diodes. *Applied physics letters*, *83*(24), 5074-5076.

[21] Bässler, H. (1993). Charge transport in disordered organic photoconductors a Monte Carlo simulation study. physica status solidi (b), 175(1), 15-56.

[22] Brütting, W. (Ed.). (2006). *Physics of organic semiconductors*. John Wiley & Sons.

[23] Flory, P. J. (1942). Thermodynamics of high polymer solutions. *The Journal of chemical physics*, *10*(1), 51-61.

[24] Huggins, M. L. (1941). Solutions of long chain compounds. *The Journal of chemical physics*, *9*(5), 440-440.

[25] Rubenstein, M., & Colby, R. H. (2003). Polymer physics: Oxford university press.

[26] Schaefer, C., Michels, J. J., & van der Schoot, P. P. A. M. (2016). Structuring of thin-film polymer mixtures upon solvent evaporation. Macromolecules, 49(18), 6858-6870.

[27] van Breemen, A., Zaba, T., Khikhlovskyi, V., Michels, J., Janssen, R., Kemerink, M., & Gelinck, G. (2015). Surface Directed Phase Separation of Semiconductor Ferroelectric Polymer Blends and their Use in Non‐Volatile Memories. Advanced Functional Materials, 25(2), 278-286.

[28] Michels, J. J., & Moons, E. (2013). Simulation of surface-directed phase separation in a solution-processed polymer/PCBM Blend. Macromolecules, 46(21), 8693-8701.

[29] Asadi, K., Wondergem, H. J., Moghaddam, R. S., McNeill, C. R., Stingelin, N., Noheda, B., ... & De Leeuw, D. M. (2011). Spinodal decomposition of blends of semiconducting and ferroelectric polymers. *Advanced Functional Materials*, *21*(10), 1887-1894.

[30] Asadi, K., Blom, P. W., & De Leeuw, D. M. (2011). The MEMOLED: Active addressing with passive driving. *Advanced Materials*, *23*(7), 865-868.

[31] Michels, J. J., van Breemen, A. J., Usman, K., & Gelinck, G. H. (2011). Liquid phase demixing in ferroelectric/semiconducting polymer blends: An experimental and theoretical study. *Journal of Polymer Science Part B: Polymer Physics*, *49*(17), 1255-1262.

[32] Keller, A. (1992). Morphology of polymers. *Pure and applied chemistry*, *64*(2), 193-204.

[33] Khikhlovskyi, V., van Breemen, A. J., Michels, J. J., Janssen, R. A., Gelinck, G. H., & Kemerink, M. (2015). 3D morphology reconstruction of nanoscale phase‐separation in polymer memory blends. *Journal of Polymer Science Part B: Polymer Physics*, *53*(17), 1231-1237.

[34] Blouin, N., Michaud, A., & Leclerc, M. (2007). A low‐bandgap poly (2, 7‐carbazole) derivative for use in high‐performance solar cells. *Advanced Materials*, *19*(17), 2295-2300.

[35] Peters, C. H., Sachs‐Quintana, I. T., Kastrop, J. P., Beaupre, S., Leclerc, M., & McGehee, M. D. (2011). High efficiency polymer solar cells with long operating lifetimes. *Advanced Energy Materials*, *1*(4), 491-494.

[36] Segalman, R. A., McCulloch, B., Kirmayer, S., & Urban, J. J. (2009). Block copolymers for organic optoelectronics. *Macromolecules*, *42*(23), 9205-9216.

[37] Lombeck, F., Di, D., Yang, L., Meraldi, L., Athanasopoulos, S., Credgington, D., ... & Friend, R. H. (2016). PCDTBT: From polymer photovoltaics to light-emitting diodes by side-chain-controlled luminescence. *Macromolecules*, *49*(24), 9382-9387.

[38] Keller, A. (1992). Morphology of polymers. *Pure and applied chemistry*, *64*(2), 193-204.

[39] Lombeck, F., Sepe, A., Thomann, R., Friend, R. H., & Sommer, M. (2016). Compatibilization of all-conjugated polymer blends for organic photovoltaics. ACS nano, 10(8), 8087-8096.

[40] Asadi, K., de Boer, T. G., Blom, P. W., & de Leeuw, D. M. (2009). Tunable Injection Barrier in Organic Resistive Switches Based on Phase-Separated Ferroelectric–Semiconductor Blends. *Advanced Functional Materials*, *19*(19), 3173-3178.

Acknowledgement

I would like to thank Prof. Dr. Andreas Walther for being my first evaluator. Also, I would like to thank Prof. Dr. Paul Blom for giving me this opportunity to work at Max-Planck Institute in his group.

I would like to express my gratitude to my project supervisor Dr. Jasper Michels for encouraging me all the time. His useful comments and suggestions from each discussion leading me to grow as a researcher.

I would also like to thank all the group members from AK Blom, Dr. Asadi Kamal, Elham Khodabakhshi, Kai Philipps, Ke Zhang, Manasvi Kumar, Saleem Anwar, Hamed Sharifi Dehsari, Anielen Halda Ribeiro, Naresh Kotadiya, Frank Keller, Verona Maus, Hans-Jürgen Guttmann, Michelle Beuchel, Christian Bauer who have shared their precious time dealing with my problems. I would like to thank Gunnar Glaßer form AK Landfester for measuring SEM for me.

Finally I would especially like to thank my parents. Without their support, I won't be able to complete my studies at University Frieburg.